



The Raman effect in crystals*

R. LOUDON

Royal Radar Establishment, Malvern, Worcs., UK

Abstract

A review is given of progress in the theoretical and experimental study of the Raman effect in crystals during the past ten years. Attention is given to the theory of those properties of long-wavelength lattice vibrations in both cubic and uniaxial crystals which can be studied by Raman scattering. In particular the phenomena observed in the Raman scattering from crystals which lack a centre of inversion are related to the theory. The angular variations of the scattering by any type of lattice vibration in a crystal having any symmetry can be easily calculated using a complete tabulation of the Raman tensor. Recent measurements of first-order lattice vibration spectra are listed. A discussion of Brillouin scattering is included. The relation of second-order Raman spectra to critical points in the lattice vibration density of states is discussed, and measurements of the second-order spectra of diamond and the alkali halides are reviewed.

The theory and experimental results for Raman scattering by electronic levels of ions in crystals are examined, and proposals for Raman scattering by spin waves, electronic excitations across the superconductive gap and by plasmons are collected together.

Finally, the prospects for applying lasers as sources for Raman spectroscopy are discussed, and progress in the new technique of stimulated Raman scattering is reviewed.

Contents	PAGE
1. Introduction	814
2. First-order Raman effect	815
2.1. Properties of long-wavelength lattice vibrations	815
2.1.1. Cubic crystals	816
2.1.2. Uniaxial crystals	818
2.1.3. Biaxial crystals	823
2.2. Theory of the scattering process	823
2.3. Selection rules and the symmetry of the scattered light	828
2.4. Extensions of the theory for piezo-electric crystals	833
2.5. Temperature effects	839
2.6. Experimental results	840
2.6.1. Piezo-electric crystals	841
2.6.2. Quartz	841
2.6.3. Alkaline-earth fluorides	842
2.6.4. Wurtzite structure crystals	842
2.6.5. Ferro-electric crystals	843
2.6.6. Rutile	844
2.7. Brillouin scattering	844
2.7.1. Theory	844
2.7.2. Experiment	846

* This article was originally published in *Advances in Physics*, volume 13, 1964. It attracted 1147 citations by October 2001, and is ranked 2 in the index of articles attracting more than 100 citations.

3.	Second-order Raman effect	846
3.1.	Theory of the scattering process	846
3.2.	Two phonon density of states and Raman selection rules	848
3.3.	Experimental results	852
3.3.1.	Diamond	852
3.3.2.	Alkali halides	853
4.	Raman scattering other than by phonons	853
4.1.	Electronic states	853
4.2.	Spin waves	854
4.3.	Superconductors	855
4.4.	Plasmons	856
5.	Recent developments	856
5.1.	Use of lasers as Raman sources	856
5.2.	Stimulated Raman effect	857
	References	860

1. Introduction

The measurement of the Raman spectrum of a crystal is one of the main methods for obtaining information about its lattice vibration frequencies. The general explanation of the Raman effect has of course been known for a long time; incident light of angular frequency ω_i can interact with the crystal to create or destroy one or more lattice vibration quanta (phonons) and the energy $\hbar\omega$ gained or lost by the lattice is compensated by a decrease or increase in the frequency ω_s of the scattered light ($\omega_s = \omega_i \mp \omega$). However, some of the more subtle effects observed in Raman scattering have only been fully understood within the past ten years with the advent of a more complete knowledge of the properties of lattice vibrations. The purpose of the present article is to review progress in the theory and measurement of the Raman effect during the past decade. For references to earlier work the review article by Menzies (1953) can be consulted. We shall ourselves refer to some of the earlier experimental work, but only where the measurements have been clarified by more recent theoretical analysis or where they are the only measurements on a particularly important substance. Other articles covering particular aspects of the subject have been written during the period under review by Bhagavantam (1953), Mathieu (1956, 1962), and Mitra (1962).

Although many new measurements of Raman spectra have been made during the past ten years, the most striking advances have been in the interpretation of measured spectra in terms of the theory of lattice vibrations, and for this reason a large part of the article is concerned with the theoretical aspects of the subject. As far as the experiments are concerned, most attention is given to the Raman spectra of those crystals whose structure is relatively simple, where theory and experiment can be most easily compared. We shall however give references to measurements on the more complex crystals, although organic crystals are completely excluded. Consideration of the ordinary Raman effect is conveniently divided into two parts; in §2 we discuss the first-order Raman effect, in which a single phonon is created or destroyed in the scattering process, while §3 is devoted to the second-order Raman effect, in which two phonons are involved. Raman scattering by excitations of the crystal other than lattice vibrations, e.g. plasmons, spin waves, etc., is dealt with in §4.

Some falling off in experimental activity is apparent when the work of the past ten years is compared with that in the decade prior to Menzies' review article. Most of the crystals easily obtainable in sufficiently good quality and size, and having

strong Raman spectra, were studied in the earlier years and the rate of progress has necessarily slowed down with the more difficult crystals left for investigation. It seems, however, that a new impetus will be given to Raman spectroscopy by the development of the optical maser, or laser. These devices provide powerful collimated beams of monochromatic radiation and appear to be ideal sources for Raman effect measurements. The frequencies of the outputs of presently available lasers extend well below the frequencies of the gas discharge emission lines of sufficient intensity for Raman work, leading to the possibility of measuring the Raman spectra of crystals (e.g. semiconductors) with electronic energy gap smaller than the present minimum of a little over 2 eV. Indeed, lasers may even prove to be more satisfactory sources than gas discharge lamps for all types of crystal. The use of lasers in Raman spectroscopy is discussed in § 5.

2. First-order Raman effect

2.1. *Properties of long-wavelength lattice vibrations*

The lattice vibrations of the majority of crystals have a maximum wavenumber which varies between about 100 cm^{-1} and 1000 cm^{-1} or higher, and first-order Raman spectra occupy a range of this extent on either side of the exciting frequency. The part of the scattered light of lower frequency than the incident light is called the Stokes component, while the part of the scattered light with higher frequency is called the anti-Stokes component. Both optic and acoustic phonons give rise to first-order Raman scattering; we consider first the optic phonons, leaving the acoustic phonons until § 2.7. Only lattice vibrations having certain types of symmetry give rise to Raman scattering; such vibrations are said to be Raman active. The phonon wave vector can take on any value lying in the Brillouin zone, the maximum value being of order π/d , where d is the lattice constant. This maximum is typically of order $3 \times 10^8\text{ cm}^{-1}$. Incident light with a wavenumber of $20\,000\text{ cm}^{-1}$ has a wave vector inside the crystal of order $2 \times 10^5\text{ cm}^{-1}$ (wave vector = $2\pi \times$ refractive index \times wavenumber) and for scattering of the light through 90° , wave vector conservation requires the wave vector of the phonon created or destroyed to be $\sim \sqrt{2} \times 2 \times 10^5\text{ cm}^{-1}$. This is small compared to π/d , and the phonons of importance in the first-order Raman effect thus have wavelengths very long compared to the lattice constant.

The smallness of the wave vector \mathbf{k} of the first-order Raman-active phonons leads to a great simplification in the discussion of their properties. There is an important distinction between those lattice vibrations which do or do not produce an electric dipole moment in the lattice, and are thus active or inactive respectively in first-order infra-red absorption. The frequencies of infra-red-inactive phonons are determined mainly by short-range forces in the lattice; phonons with wavelength long compared to the lattice constant are not influenced by the dispersive effects of these forces and have essentially the same frequency as infinite wavelength phonons. The Raman shifts thus measure the phonon frequencies at $\mathbf{k} = 0$, and no variation in the Raman shift is produced by variation of the scattering angle or of the relative orientation of the light beams and the crystal axes. However, for infra-red-active phonons, the accompanying long-range electric fields lead to shifts of the frequencies of some of the Raman-active phonons away from their $\mathbf{k} = 0$ values, to a lifting of some of the phonon branch degeneracies, to a variation of frequency with the direction of the phonon wave vector \mathbf{k} in non-cubic crystals, and to other effects which are

considered in later sections. A phonon can be simultaneously Raman and infra-red-active only in crystal structures which lack a centre of inversion, i.e. piezo-electric crystals. It is convenient to divide up the discussion of the properties of long-wavelength infra-red-active phonons into three parts corresponding to the three main types of crystal symmetry.

2.1.1. Cubic crystals

Huang (1951) has treated the properties of the long-wavelength optic vibrations of a polar diatomic lattice having cubic symmetry (see also Born and Huang 1954). He shows that in the presence of an optic vibration of the lattice having frequency ω , the electric field \mathbf{E} and relative displacement \mathbf{r} of the positive and negative sub-lattices are related by the macroscopic equations:

$$(\omega_0^2 - \omega^2)\mathbf{r} = \left(\frac{V}{4\pi M}\right)^{1/2} (\epsilon^0 - \epsilon)^{1/2} \omega_0 \mathbf{E}, \quad (1)$$

$$\mathbf{P} = \left(\frac{M}{4\pi V}\right)^{1/2} (\epsilon^0 - \epsilon)^{1/2} \omega_0 \mathbf{r} + (\epsilon - 1) \frac{\mathbf{E}}{4\pi}, \quad (2)$$

where \mathbf{P} is the polarization, ω_0 is the lattice dispersion frequency, ϵ and ϵ^0 are the optical and static dielectric constants, V is the crystal volume and M is the reduced mass of the two sub-lattices. The effect of anharmonic damping is not included in (1) and (2), and in order for these equations to be valid the inverse phonon relaxation times due to anharmonicity must be small compared to the frequencies of the phonons and the separations between adjacent phonon branches. If the vibration is assumed to have plane-wave form with spatial dependence $\exp(i\mathbf{k} \cdot \mathbf{R})$, then Maxwell's equations impose the requirement:

$$\mathbf{E} = \frac{-4\pi[\mathbf{k}(\mathbf{k} \cdot \mathbf{P}) - \omega^2 \mathbf{P}/c^2]}{k^2 - \omega^2/c^2}. \quad (3)$$

All the properties of the long-wavelength optic excitations of the crystal can be derived from (1), (2) and (3). For the transverse solutions, $\mathbf{k} \cdot \mathbf{P} = 0$, and elimination of \mathbf{r} , \mathbf{E} and \mathbf{P} from the equations gives:

$$\frac{k^2 c^2}{\omega^2} = \frac{\omega_0^2 \epsilon^0 - \omega^2 \epsilon}{\omega_0^2 - \omega^2}. \quad (4)$$

For the longitudinal solution $\mathbf{k} \cdot \mathbf{P} = kP$, leading to:

$$\omega = \omega_0 \left(\frac{\epsilon^0}{\epsilon}\right)^{1/2} = \omega_l \quad \text{say}. \quad (5)$$

The schematic form of the ω versus k curves is illustrated in figure 1, where the numbers in parentheses indicate the branch degeneracy, and L and T denote longitudinal and transverse polarizations. In the region where both $\omega < \sim 2\omega_0$ and $k < \sim 2\omega_0(\epsilon^0)^{1/2}/c$, the transverse vibrations are a mixture of lattice oscillation and electromagnetic wave, i.e. the modes are part phonon and part photon. Outside this region, for $\omega > \sim 2\omega_0$ the transverse vibrations are purely photons (modified to some extent by the higher frequency electronic states of the crystal), while the transverse excitations having $\omega = \omega_0$ are purely mechanical oscillations of the lattice having no photon component. Since the phonons which cause right-angle Raman scattering

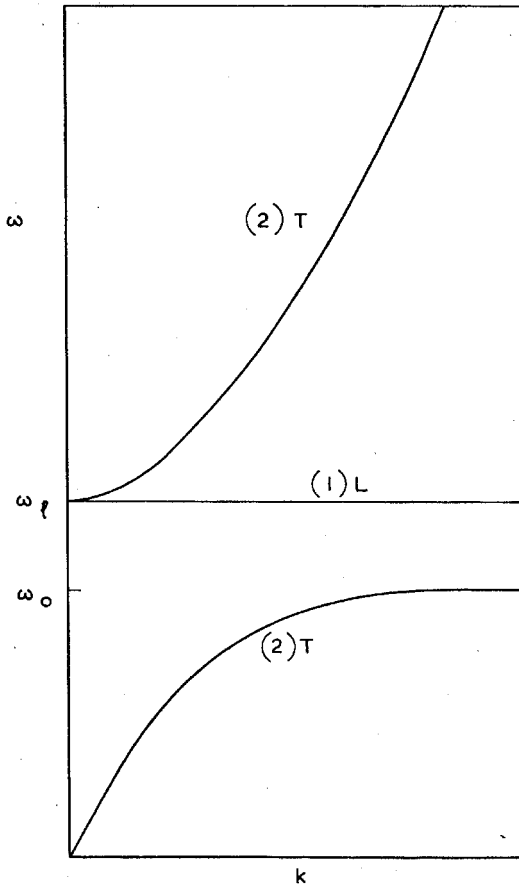


Figure 1. Phonon dispersion curves at small wave vector in a cubic diatomic lattice.

typically have a wave vector \mathbf{k} of order $3 \times 10^5 \text{ cm}^{-1}$ and an angular frequency ω of order $2 \times 10^{14} \text{ sec}^{-1}$, \mathbf{k} and ω satisfy the inequality $k \gg \omega/c$. The phonons of interest thus lie off the right-hand edge of figure 1 in the region where the transverse phonons have the constant frequency ω_0 . Both the longitudinal and transverse phonons can be Raman active, leading in general to two Stokes and two anti-Stokes peaks in the Raman spectrum, separated from the exciting frequency by amounts of magnitude ω_l and ω_0 . The frequencies ω_l and ω_0 are related by (5), a well-known relation first derived by Lyddane *et al.* (1941). At $\mathbf{k} = 0$ the optic branches have a threefold degeneracy with frequency ω_l , although for a finite crystal of dimension L the effect of the long-range electric fields interacting with the sample boundaries may perturb the frequencies of the phonons having wave vector of order, and smaller than $1/L$, and figure 1 is unreliable in this region.

The electric field strengths associated with the Raman-active phonons can be obtained by substituting the appropriate values of ω into (1). For the transverse phonons, $\omega = \omega_0$ and $E = 0$; for the longitudinal phonons $\omega = \omega_l$ and

$$\mathbf{E} = -\left(\frac{4\pi M}{V}\right)^{1/2} \omega_l \left(\frac{1}{\epsilon} - \frac{1}{\epsilon^0}\right)^{1/2} \mathbf{r}. \quad (6)$$

The mean square amplitude of the relative sub-lattice displacement \mathbf{r} due to a lattice vibration of frequency ω is:

$$\langle r^2 \rangle = (2n + 1)\hbar/2M\omega, \quad (7)$$

where n is the number of phonons contributing to the vibration; in thermal equilibrium:

$$n = [\exp(\hbar\omega/k_B T) - 1]^{-1}, \quad (8)$$

where k_B is Boltzmann's constant and T is the temperature.

The above theory applies directly to a polar diatomic lattice; the zinc blende structure is an example of a crystal with two atoms in the unit cell whose optic vibrations are both Raman and infra-red active. For crystals with more than two atoms in the unit cell but still having only one infra-red-active vibration (e.g. CaF_2), the results continue to hold, but where more than one vibration is infra-red active the theory must be extended. We do not pursue this case in any detail, except to quote an extension of the Lyddane–Sachs–Teller relation (5) due to Cochran and Cowley (1962). This applies in its most general form to a crystal of any symmetry having any number of infra-red-active branches. For a cubic crystal having N infra-red-active vibrations with longitudinal and transverse frequencies $\omega_L(j)$ and $\omega_T(j)$ ($j = 1, 2, \dots, N$) the generalization of (5) is:

$$\prod_{j=1}^N \left[\frac{\omega_L(j)}{\omega_T(j)} \right]^2 = \frac{\epsilon^0}{\epsilon}. \quad (9)$$

2.1.2. Uniaxial crystals

Merten (1960) and Loudon (1963a) have treated some of the properties of long-wavelength lattice vibrations in uniaxial crystals. The treatment is based on a generalization of Huang's equations for a cubic crystal given in the previous subsection. We consider a uniaxial crystal in which only one group of three lattice vibration branches is infra-red active, for example the wurtzite structure. Due to the anisotropy of the crystal, in the absence of long-range electric forces the vibration in which the atoms are displaced parallel to the c -axis has a frequency ω_{\parallel} which is different to the frequency ω_{\perp} of the two degenerate vibrations in which the atomic displacements lie perpendicular to the c -axis, in the ab -plane. The number of high and low frequency dielectric constants is correspondingly doubled. The phonon spectrum is obtained by writing down pairs of equations similar to (1) and (2) for the components of oscillation parallel and perpendicular to the c -axis. Equation (3) continues to hold since it is derived directly from Maxwell's equations, with no assumptions about the crystal structure; it can be divided into two equations for the components of \mathbf{E} parallel and perpendicular to the c -axis. This gives a total of six equations, enabling elimination of the two components each of \mathbf{r} , \mathbf{P} and \mathbf{E} . For any relative orientation of the phonon wave vector \mathbf{k} and the c -axis, the equations have a solution in which \mathbf{E} and \mathbf{P} are perpendicular to both \mathbf{k} and the c -axis. This corresponds to the ordinary wave, and leads to:

$$\frac{k^2 c^2}{\omega^2} = \frac{\omega_{\perp}^2 \epsilon_{\perp}^0 - \omega^2 \epsilon_{\perp}}{\omega_{\perp}^2 - \omega^2} \quad (\text{ordinary wave}). \quad (10)$$

The other solutions correspond to the extraordinary waves, and **E** and **P** do not in general have any simple orientation relative to **k** and the *c*-axis (although the displacement **D** is perpendicular to **k**). The frequencies of the extraordinary waves depend on the angle θ between **k** and the *c*-axis:

$$\frac{k^2 c^2}{\omega^2} = \frac{\left[\frac{\omega_{\parallel}^2 \epsilon_{\parallel}^0 - \omega^2 \epsilon_{\parallel}}{\omega_{\parallel}^2 - \omega^2} \right] \left[\frac{\omega_{\perp}^2 \epsilon_{\perp}^0 - \omega^2 \epsilon_{\perp}}{\omega_{\perp}^2 - \omega^2} \right]}{\left[\frac{\omega_{\parallel}^2 \epsilon_{\parallel}^0 - \omega^2 \epsilon_{\parallel}}{\omega_{\parallel}^2 - \omega^2} \right] \cos^2 \theta + \left[\frac{\omega_{\perp}^2 \epsilon_{\perp}^0 - \omega^2 \epsilon_{\perp}}{\omega_{\perp}^2 - \omega^2} \right] \sin^2 \theta}$$

(extraordinary waves). (11)

Notice that for $\theta = 0$ (propagation parallel to the *c*-axis) (11) reduces to (10), and that (11) reduces to (4) when the distinction between \parallel and \perp quantities is removed.

It is convenient to define two frequencies:

$$\omega'_{\parallel} = \omega_{\parallel} \left(\frac{\epsilon_{\parallel}^0}{\epsilon_{\parallel}} \right)^{1/2} \quad \text{and} \quad \omega'_{\perp} = \omega_{\perp} \left(\frac{\epsilon_{\perp}^0}{\epsilon_{\perp}} \right)^{1/2}$$
(12)

analogous to ω_l defined by (5) for cubic crystals. Reference to (10) and (11) shows that for **k** = 0 the phonon frequencies are ω'_{\parallel} (singlet) and ω'_{\perp} (doublet). The Raman-active vibrations have $k \gg \omega/c$ as before, and (10) and (11) show that the Raman frequencies are given by:

$$\omega = \omega_{\perp} \quad (\text{ordinary phonon}),$$
(13)

and

$$\left[\frac{\omega_{\parallel}^2 \epsilon_{\parallel}^0 - \omega^2 \epsilon_{\parallel}}{\omega_{\parallel}^2 - \omega^2} \right] \cos^2 \theta + \left[\frac{\omega_{\perp}^2 \epsilon_{\perp}^0 - \omega^2 \epsilon_{\perp}}{\omega_{\perp}^2 - \omega^2} \right] \sin^2 \theta = 0 \quad (\text{extraordinary phonons}).$$
(14)

Equation (14) is a quadratic for ω^2 , having in general two distinct roots, and the ordinary and extraordinary phonons together contribute three Stokes (and three anti-Stokes) lines to the Raman spectrum, except for certain special orientations of the crystal. If ω_1^2 and ω_2^2 are the two roots of (14), it is easy to show that they satisfy a modified Lyddane–Sachs–Teller relation:

$$\frac{\omega_1^2 \omega_2^2}{\omega_{\parallel}^2 \omega_{\perp}^2} = \frac{\epsilon_{\parallel}^0 \cos^2 \theta + \epsilon_{\perp}^0 \sin^2 \theta}{\epsilon_{\parallel} \cos^2 \theta + \epsilon_{\perp} \sin^2 \theta}.$$
(15)

The electric field strength associated with a Raman-active phonon is given by the generalizations of (1) with the appropriate value of ω substituted. The ordinary phonon has zero electric vector and so also does an extraordinary phonon when θ is such as to make its frequency either ω_{\parallel} or ω_{\perp} (this can occur only for $\theta = 0$ or 90°). Equation (3) shows that **E** is parallel to **k** for the extraordinary phonons (when $k \gg \omega/c$).

Rather than discuss (14) for general values of the frequencies and dielectric constants, it is more convenient to consider two limiting cases which correspond to many crystals of experimental interest.

(i) $|\omega_{\parallel} - \omega_{\perp}| \ll \omega'_{\parallel} - \omega_{\parallel}$ and $\omega'_{\perp} - \omega_{\perp}$. In this case, the difference in frequency of vibrations parallel and perpendicular to the *c*-axis, caused by anisotropy of the force constants, is small compared to the difference between the frequencies with and

without the l superscript, which is caused by electrostatic forces. Hexagonal ZnO and SiC are examples of crystals where this limit holds (see §2.6). For $\theta = 0$ the two solutions of (14) are ω_{\perp} and ω'_{\parallel} , while for $\theta = 90^{\circ}$ the solutions are ω_{\parallel} and ω_{\perp} . For general values of θ , one root of (14) lies in the vicinity of ω_{\parallel} and ω_{\perp} while the second root is close to ω'_{\parallel} and ω'_{\perp} . Using the assumed inequalities satisfied by the characteristic frequencies and assuming, in addition that the percentage difference between ϵ_{\parallel} and ϵ_{\perp} is small, the two solutions of (14) are approximately:

$$\omega^2 = \omega_{\parallel}^2 \sin^2 \theta + \omega_{\perp}^2 \cos^2 \theta \quad (16)$$

and

$$\omega^2 = \omega_{\parallel}^{\prime 2} \cos^2 \theta + \omega_{\perp}^{\prime 2} \sin^2 \theta. \quad (17)$$

The complete dispersion curves in this limit are plotted in figure 2 for three directions of propagation. The relative values of the frequencies and dielectric constants have been chosen arbitrarily for a negative uniaxial crystal. The frequencies of the Raman-active phonons given by (13) and (14), and approximately by (16) and (17), are associated with the phonons at the right-hand edges of the graphs where the branches are flat. The extraordinary branches have strictly no simple polarization except for $\theta = 0$ and 90° . However the predominance of electrostatic forces over the anisotropy in the interatomic forces ensures that the departures of the upper phonon branch from longitudinal polarization, and of the lower branch from transverse polarization, are small. The electric field associated with the upper branch is of the same order as that in cubic crystals given by (6), while the electric field associated with the lower branch is much smaller, roughly by a factor $[(\omega_{\parallel}^2 - \omega_{\perp}^2)/(\omega_{\parallel}^{\prime 2} - \omega_{\perp}^{\prime 2})]$. The anisotropy in the infra-red properties of this type of crystal is small.

(ii) $|\omega_{\parallel} - \omega_{\perp}| \gg \omega'_{\parallel} - \omega_{\parallel}$ and $\omega'_{\perp} - \omega_{\perp}$. For this case, one solution of (14) always lies in the vicinity of ω_{\parallel} and ω'_{\parallel} and the other solution always lies in the vicinity of ω_{\perp} and ω'_{\perp} . Approximate solutions of (14), obtained as before, are:

$$\omega^2 = \omega_{\parallel}^2 \sin^2 \theta + \omega_{\parallel}^{\prime 2} \cos^2 \theta, \quad (18)$$

$$\omega^2 = \omega_{\perp}^2 \cos^2 \theta + \omega_{\perp}^{\prime 2} \sin^2 \theta. \quad (19)$$

Dispersion curves in this limit for three directions of propagation are plotted in figure 3. As θ is increased from 0 to 90° , the upper extraordinary branch changes from longitudinal to transverse polarization, while the lower branch changes from transverse to longitudinal. For intermediate values of θ the extraordinary branches have strictly no simple polarization, although the predominance of the anisotropy in the interatomic forces over the long-range electric forces causes the relative sublattice displacement \mathbf{r} in the upper phonon branch to be almost parallel to the c -axis, with the displacement in the lower branch approximately perpendicular to the c -axis, for all values of θ . Since only a transversely polarized phonon can be infra-red active, there is considerable anisotropy in the infra-red properties of this type of crystal.

Formulae equivalent to (18) and (19) were first derived by Poulet (1952, 1955), and Ketelaar *et al.* (1954) have given a theory of the variation with θ of the intensity and frequency of the reflection from a uniaxial crystal. Observations of the variation with θ of the frequency of the maximum of a reflection band have been made by Couture-Mathieu *et al.* (1952a,b) on crystals of quartz, lithium perchlorate ($\text{LiClO}_4 \cdot 3\text{H}_2\text{O}$) and iodic acid (IO_3H). All these crystals appear to satisfy the

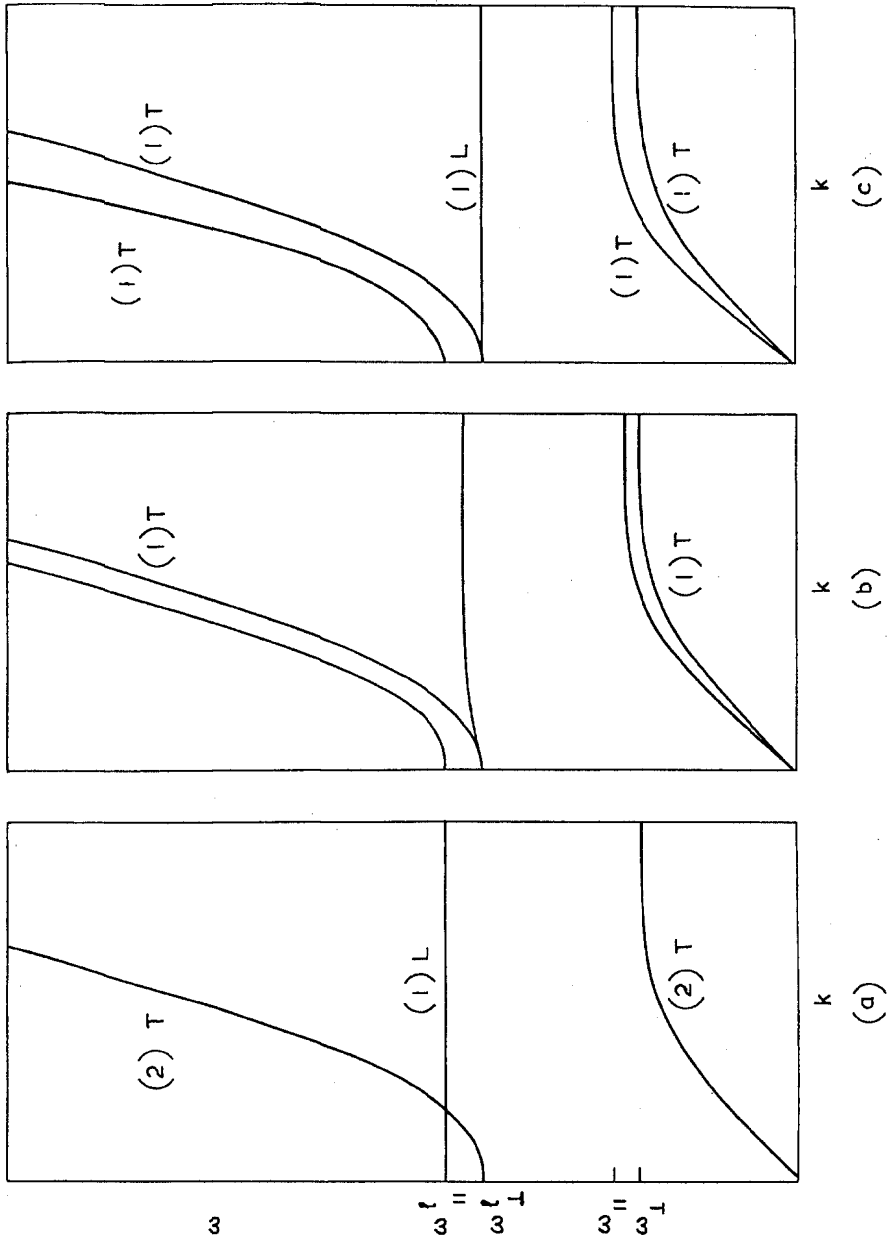


Figure 2. Phonon dispersion curves at small wave vector in a uniaxial crystal for which electrostatic forces predominate over anisotropy in the interatomic forces. Phonon wave vector (a) parallel to c -axis, (b) in intermediate direction and (c) lying in the ab -plane.

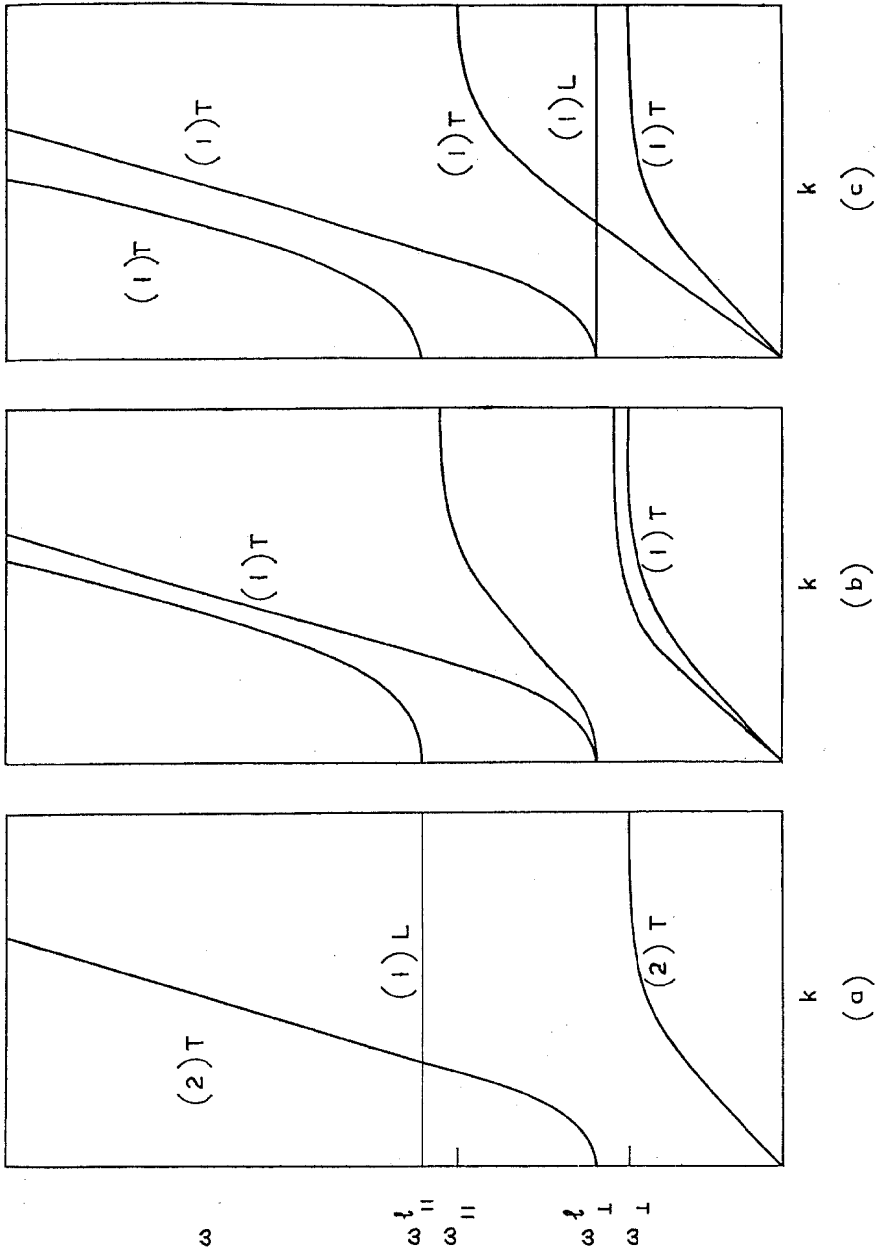


Figure 3. Phonon dispersion curves at small wave vector in a uniaxial crystal for which anisotropy in the interaction forces predominates over electrostatic forces. Phonon wave vector (*a*) parallel to *c*-axis, (*b*) in intermediate direction and (*c*) lying in the *ab*-plane.

frequency inequality assumed in this sub-section, although the inequality is only weakly satisfied in the case of quartz. In any case, the maximum in the reflection band does not occur exactly at the phonon frequency ω , so that the above measurements cannot be closely related to the theory without more detailed calculations of the shape of the reflection band. Some progress in this direction has been made by Ketelaar *et al.* (1954) who compared their theory with experiments on sodium nitrate (NaNO_3). A much more direct comparison of the theory of this section with experiment can be made for the results on the variation of Raman frequency with θ (see §2.6). Mention may also be made of the work of Tramer (1959a,b), who observed the variation of phonon frequency with θ in sodium nitride (NaN_2) by direct absorption measurements as well as by the Raman effect. Reviews of the relevant infra-red and Raman results in this field have been given by Haas (1956) and Mathieu *et al.* (1960).

Expressions for the electric fields associated with the upper and lower phonon branches in figure 3 can be derived from the generalizations of (1), (2) and (3), using (12), (18) and (19):

$$\mathbf{E} = -\left(\frac{4\pi M}{V}\right)^{1/2} \omega'_{\parallel} \cos \theta \left(\frac{1}{\epsilon_{\parallel}} - \frac{1}{\epsilon_{\parallel}^0}\right)^{1/2} r_{\parallel} \hat{\mathbf{k}} \quad (\text{upper branch}), \quad (20)$$

$$\mathbf{E} = -\left(\frac{4\pi M}{V}\right)^{1/2} \omega'_{\perp} \sin \theta \left(\frac{1}{\epsilon_{\perp}} - \frac{1}{\epsilon_{\perp}^0}\right)^{1/2} r_{\perp} \hat{\mathbf{k}} \quad (\text{lower branch}), \quad (21)$$

where r_{\parallel} and r_{\perp} are the components of \mathbf{r} parallel and perpendicular to the c -axis and $\hat{\mathbf{k}}$ is a unit vector parallel to \mathbf{k} . These values for the field strength will be used in calculating the Raman scattering intensity. Expressions equivalent to (20) and (21) have been derived by Poulet (1955). Our choice for the relative magnitude of ω_{\parallel} and ω_{\perp} is of course arbitrary; for many crystals ω_{\parallel} is smaller than ω_{\perp} .

The theory of this sub-section ceases to be valid when more than one group of three lattice vibrations is infra-red active. There is little theoretical work on the properties of the lattice vibrations in this situation, although the generalizations of the Lyddane–Sachs–Teller relation due to Cochran and Cowley (1962) continue to apply. For a group of infra-red-active phonons which is well separated from the remaining groups, the variations of their frequencies with θ may still be represented by equations similar to (18) and (19), but the constants occurring in them are not related to the dielectric constants by (12).

2.1.3. Biaxial crystals

There is little work, either theoretical or experimental, on the Raman effect in biaxial crystals. The long-wavelength properties could be determined by writing down equations similar to (1) and (2) for the components of oscillation in the directions of the three principal axes. The frequencies of the three Raman-active phonons are determined by a cubic equation in ω^2 and they all vary with direction of propagation.

2.2. Theory of the scattering process

Each elementary Raman scattering event involves the destruction of a photon of frequency ω_i , incident from a light source, the creation of a scattered photon of frequency ω_s , and the creation or destruction of a phonon of frequency ω . We choose

to concentrate on the Stokes component of the scattering, so that $\omega_i = \omega_s + \omega$; the properties of the anti-Stokes component can always be obtained by simple substitutions. Figure 4 illustrates three different Raman scattering processes in terms of the elementary interactions between the radiation, the electrons and the lattice; H_{EL} , $H_{RL}^{(1)}$ and H_{ER} represent, in an obvious notation, the first-order interactions between the three systems. The three-phonon anharmonic interaction H_A and the second-order moment radiation-lattice interaction $H_{RL}^{(2)}$ (see Lax and Burstein 1955) are higher-order interactions. The initial state, with photon ω_i present, occurs at the left-hand end of each diagram, and the final state, with photon ω_s and phonon ω present, occurs on the right. It is possible to envisage more complicated processes connecting the initial and final states, but these are all of higher order and give a smaller contribution to the scattering. It is noted that processes 4(b) and 4(c) require the existence of infra-red-active phonons, and could therefore not take place in a homopolar crystal, e.g. diamond. Indeed, numerical estimates indicate that even when all three processes are allowed, 4(a) dominates 4(b) and 4(c) in scattering intensity, and most theoretical work on Raman scattering has explicitly assumed that the radiation interacts with the lattice vibrations through the intermediary of the electrons in the crystal.

Expressed in words, process 4(a) involves three virtual electronic transitions accompanied by the following photon and phonon transitions: (1) a photon ω_i is absorbed, (2) an optic phonon ω is created, (3) a photon ω_s is emitted. The scattering crystal is generally in its electronic ground state, with all valence bands full and all

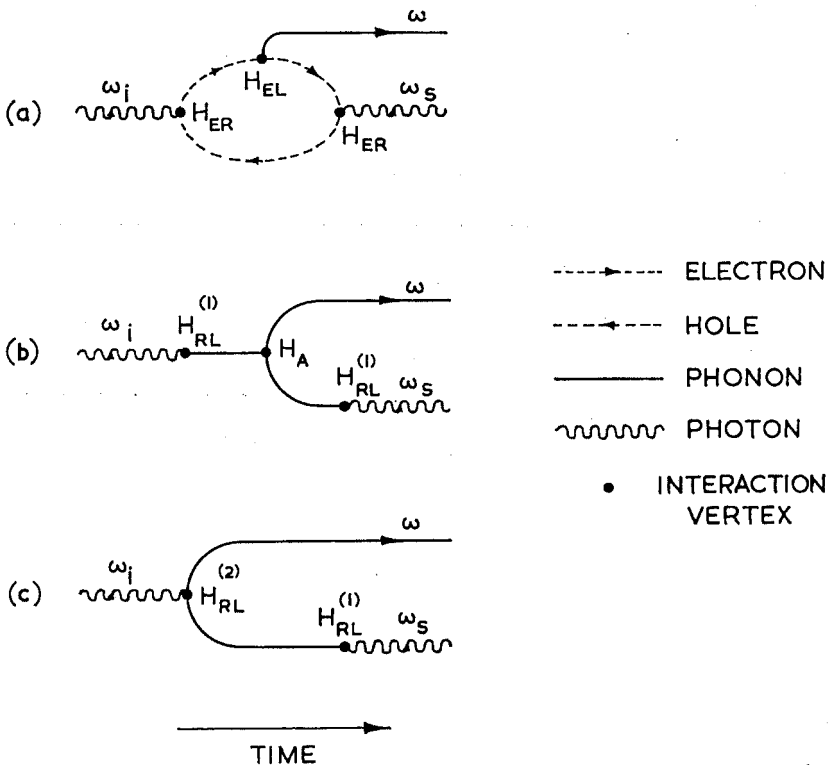


Figure 4. Three types of elementary Raman scattering process.

conduction bands empty, at the start of the scattering process, and it returns to its electronic ground state at the end of the event. The virtual intermediate states involve the excitation of electron-hole pairs. The three transitions can occur in any time order, leading to six related processes which could be illustrated by deforming figure 4(a) to change the relative order of the transition vertices.

The problem of calculating the scattering intensity due to the basic process 4(a) has been tackled in a variety of ways. The first systematic treatment of optic-phonon Raman scattering in crystals was given by Born and Bradburn (1947) and the same approach has subsequently been used in further work by Born and his collaborators (Smith 1948, Theimer 1951, Born and Huang 1954). In this approach, which makes use of the semi-classical radiation theory, the intensity of the scattered radiation is arrived at by calculating the electric moment \mathbf{M} set up in the crystal by the electric vector $\text{Re}[\mathbf{E} \exp(-i\omega t)]$ of the incident light beam. If the polarizability tensor associated with the electrons in the crystal is $\alpha_{\rho\sigma}$, then

$$M_\rho = \sum_\sigma \alpha_{\rho\sigma} E_\sigma. \quad (22)$$

The scattered light is produced by re-radiation of energy by the oscillating dipole moment \mathbf{M} , the scattered intensity being proportional to $|\mathbf{M}|^2$ and inversely proportional to the fourth power of the wavelength of the scattered light. The quantum-mechanical expression for the electronic polarizability tensor $\alpha_{\rho\sigma}$ involves the energy eigenvalues and wave-functions of the electron system (see Born and Huang 1954). Because of the existence of the electron-lattice interaction H_{EL} , the electronic eigenvalues and wave-functions in a diatomic lattice depend on the relative displacement amplitude \mathbf{r} of the two sub-lattices, and the electronic polarizability can be expanded in a power series in \mathbf{r} :

$$\alpha_{\rho\sigma} = \alpha_{\rho\sigma}^{(0)} + \sum_\mu \alpha_{\rho\sigma,\mu} r_\mu + \sum_{\mu,\nu} \alpha_{\rho\sigma,\mu\nu} r_\mu r_\nu + \text{O}(r^3), \quad (23)$$

where

$$\alpha_{\rho\sigma,\mu} = \left(\frac{\partial \alpha_{\rho\sigma}}{\partial r_\mu} \right)_{r=0} \quad \text{and} \quad \alpha_{\rho\sigma,\mu\nu} = \left(\frac{\partial^2 \alpha_{\rho\sigma}}{\partial r_\mu \partial r_\nu} \right)_{r=0}. \quad (24)$$

The term linear in r gives rise to the first-order Raman scattering, the quadratic term gives rise to second-order Raman scattering, and so on. The forms of the terms which occur in the expansion have been discussed by Born and Huang (1954).

The Born and Bradburn method has been applied to first-order Raman scattering in diamond by Smith (1948). The square of the relative displacement amplitude caused by a single optic phonon in diamond is given by 7:

$$\langle r^2 \rangle = \hbar/2M\omega_0, \quad (25)$$

where ω_0 is the optic phonon frequency. Consider the scattering geometry shown in figure 5, where x , y and z are orthogonal axes which coincide with principal axes of the crystal and \mathbf{k}_i , \mathbf{k}_s and \mathbf{k} are the wave vectors of the incident light, scattered light and phonon respectively. Energy and wave vector conservation lead to:

$$\omega_i = \omega_s + \omega_0, \quad (26)$$

$$\mathbf{k}_i = \mathbf{k}_s + \mathbf{k}. \quad (27)$$

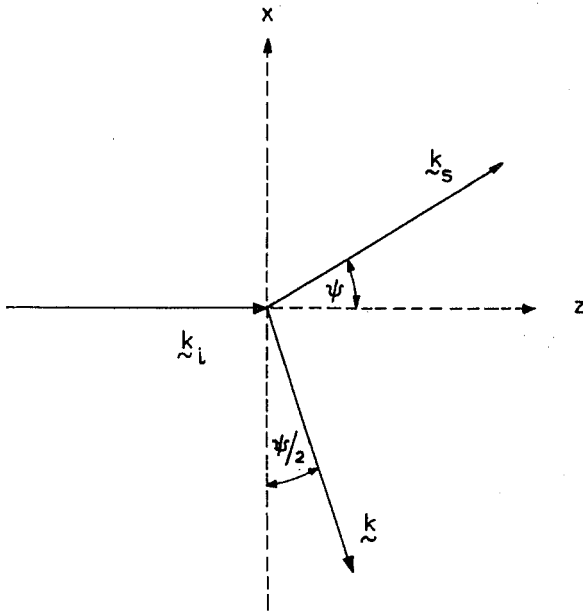


Figure 5. Raman scattering geometry.

Since the percentage difference between ω_i and ω_s is small, $|\mathbf{k}_i|$ and $|\mathbf{k}_s|$ are not very different and they have been assumed equal in calculating the phonon direction. This approximation leads to:

$$k = 2k_i \sin(\psi/2). \quad (28)$$

Smith considers the case of right-angle scattering where $\psi = 90^\circ$. We define the Raman scattering efficiency S to be the ratio of the number of scattered photons ω_s produced per unit time per unit cross-sectional area of the crystal in solid angle $d\Omega$ about the direction of observation to the number of incident photons ω_i crossing unit area in unit time. Smith has investigated the symmetry properties of $\alpha_{\rho\sigma\mu}$ and finds that the only non-vanishing components of the tensor are those for which ρ , σ and μ refer to different crystal axes. This leaves three distinct components (the tensor is symmetrical with respect to interchange of ρ and σ because it is derived from the symmetrical polarizability tensor $\alpha_{\rho\sigma}$) which are all equal. The result of Smith for the first-order Raman scattering efficiency with unpolarized incident light and unanalysed scattered light is:

$$S = \frac{3\hbar\omega_s^4 L d\Omega}{\rho c^4 \omega_0} |\alpha_{zy,x}|^2 (n_0 + 1), \quad (29)$$

where L is the length of the crystal in the direction of \mathbf{k}_i , ρ is the crystal density and n_0 is the Bose population factor. The expression for the anti-Stokes component has $n_0 + 1$ replaced by n_0 .

A more direct way of obtaining the Raman scattering tensor is to treat the three-step scattering process illustrated in figure 4(a) by third-order time-dependent perturbation theory, and this calculation has been performed by Loudon (1963b) for the particular cases of diamond and zinc blende structure crystals. In this

approach, which uses second quantization of the radiative field, the quantity calculated is the probability per unit time $1/\tau$ that one of the incident photons is destroyed in a Raman scattering process, given by the usual third-order expression:

$$\frac{1}{\tau} = \frac{2\pi}{\hbar^6} \sum_{\mathbf{k}, \mathbf{k}_s} \left| \sum_{a,b} \frac{\langle n_i - 1, 1; n_0 + 1; 0 | H_I | \alpha \rangle \langle a | H_I | b \rangle \langle b | H_I | n_i, 0; n_0; 0 \rangle}{(\omega_a - \omega_i)(\omega_b - \omega_i)} \right|^2 \times \delta(\omega_i - \omega_0 - \omega_s), \quad (30)$$

where n_i , 0 and n_0 are the numbers of incident photons, scattered photons and optic phonons present in the initial state, a and b run over complete sets of intermediate states for the whole system, the summation over \mathbf{k}_s includes only directions within the solid angle $d\Omega$, and $H_I = H_{ER} + H_{EL}$. The H_{ER} part contributes in two of the matrix elements while it is the H_{EL} part which contributes in the third matrix element. The final zeros in the initial and final state quantum numbers indicate that the electrons are in their ground state before and after the scattering event. Evaluating the summations and the matrix elements, (30) leads to the following expression for the scattering efficiency assuming the same geometry as Smith:

$$S = \frac{L\epsilon^{1/2}}{\tau n_i c} = \frac{e^4 \omega_s V (n_0 + 1) L d \Omega}{4 \hbar^3 m^4 d^2 M c^4 \omega_0 \omega_i} [|R_{yz}^x|^2 + |R_{xy}^z|^2 + |R_{xz}^y|^2], \quad (31)$$

where e and m are the electronic charge and mass, d is the lattice constant and V is the crystal volume. The three components of the tensor R are equal for diamond or zinc blende structure crystals, and are given by expressions of the form:

$$R_{yz}^x = R_{yz}^x(-\omega_i, \omega_s, \omega_0) = \frac{1}{V} \sum_{\alpha, \beta} \left\{ \frac{P_{0\beta}^z \Xi_{\beta\alpha}^x P_{\alpha 0}^y}{(\omega_\beta + \omega_0 - \omega_i)(\omega_\alpha - \omega_i)} + \text{five similar terms} \right\}, \quad (32)$$

where the subscripts on the p and Ξ matrix elements refer to electron-hole pair states with energies $\hbar\omega_\alpha$ and $\hbar\omega_\beta$, 0 referring to the electronic ground state. The two subscripts on R are the polarization directions of the incident and scattered photons respectively while the superscript is the direction of polarization of the phonon. The explicit term on the right-hand side of (32) arises from the order of interaction vertices drawn in figure 4(a), and the remaining five terms correspond to the other possible diagrams obtainable by rearrangement of this order. The two matrix elements of the electronic momentum operator p arises from the two H_{ER} matrix elements. The electron-lattice interaction H_{EL} has been treated in the deformation potential approximation (Bir and Pikus 1961, Whitfield 1961) and the Ξ matrix elements are deformation potentials.

The signs attached to the frequencies in R_{yz}^x on the right-hand side of (32) have been chosen so that a negative (positive) frequency corresponds to destruction (creation) of the appropriate photon or phonon. Whereas the analogous quantity $\alpha_{\rho\sigma,\mu}$ used in the Born theory of Raman scattering was invariant under interchange of the polarizations ρ and σ of the scattered and incident photons, R_{yz}^x does not in general have the corresponding property. Instead, inspection of the complete form of the tensor shows that it satisfies:

$$R_{yz}^x(-\omega_i, \omega_s, \omega_0) = R_{zy}^x(-\omega_i + \omega_0, \omega_s + \omega_0, -\omega_0). \quad (33)$$

However, when ω_0 is sufficiently small that it can be neglected in comparison with all the other frequencies occurring in the tensor, as is usually the case, (33) becomes:

$$R_{yz}^x(-\omega_i, \omega_i, 0) = R_{zy}^x(-\omega_i, \omega_i, 0) \quad (34)$$

and R_{yz}^x has the same symmetry properties as $\alpha_{zy,x}$. Indeed, explicit calculation of $\alpha_{zy,x}$ using the deformation potential electron-lattice interaction and the well-known quantum-mechanical form of the polarizability tensor, gives:

$$\alpha_{zy,x} = -\frac{e^2}{m^2\omega_i^2\hbar^2d} R_{yz}^x(-\omega_i, \omega_i, 0). \quad (35)$$

Thus for diamond, where $\rho = 4M/V$, (29) and (31) become identical in the small ω_0 limit. Numerical estimates based on (31) indicate that Raman scattering efficiencies may typically be of order 10^{-6} or 10^{-7} .

The interaction H_{ER} between the radiation, having electric field \mathbf{E} and vector potential \mathbf{A} , and the electrons, having position \mathbf{x} and momentum \mathbf{p} , can be represented either as $-e\mathbf{E} \cdot \mathbf{x}$ or as $-e\mathbf{A} \cdot \mathbf{p}/mc$. For Raman scattering from molecules, both representations lead to the same results for the scattering tensor, contrary to an assertion by Kondilenko *et al.* (1960) (see the correction by Kondilenko and Strizhevskii 1961). However, for scattering by crystals the matrix elements of \mathbf{x} have complicated properties due to the fact that the electronic wave functions extend throughout the crystal (see Blount 1963 and the conclusion of Butcher and McLean 1963) and it is more satisfactory to use the $-e\mathbf{A} \cdot \mathbf{p}/mc$ representation, even though this leads to formulae which do not explicitly show the dependence of the scattered intensity on the fourth power of the wavelength (cf. (29), (31) and (35)).

Strizhevskii (1962) has considered the theory of Raman scattering in non-cubic crystals. He treats the quantization of the radiative field in an anisotropic crystal and derives a formula for the scattered light intensity which is sufficiently general in form to apply to scattering by phonons, impurities, lattice defects, etc. As a result of this generality it is difficult to draw any explicit conclusions from his formula.

2.3. Selection rules and the symmetry of the scattered light

The different long-wavelength phonon branches in a given crystal correspond to different symmetries of vibration of the atoms in the unit cell and are characterized by irreducible representations of the space group of the crystal lattice. If the wavelengths of the Raman phonons are assumed to be effectively infinite, then the crystal point group can be used in classifying the phonon symmetries. This infinite wavelength assumption is not valid for Raman-active phonons which are also infra-red active, as is evident from the discussion of §2.1, and this type of vibration will be discussed separately in the following section.

The selection rules for Raman-active phonons can be determined by standard group-theoretical methods and the calculation is described in some detail by Heine (1960), who bases his work on the polarizability derivative theory of Born and Bradburn (1947) described in the previous section (see also Theimer 1953). The result of this approach is that a phonon can participate in a first-order Raman transition if and only if its irreducible representation is the same as one of the irreducible representations which occur in the reduction of the representation of the polarizability tensor. The irreducible representations by which the components of the

polarizability tensor transform are conveniently listed by Herzberg (1945) and Wilson *et al.* (1955) for the set of molecular point groups, which includes the 32 crystal point groups. Mathieu (1945) has listed the Raman-active vibrational symmetries for the different crystal classes. Many of the results had been given at an earlier date by Bhagavantam and Venkatarayudu (1939) who considered several particular crystals in detail.

The intensity of the Raman-scattered radiation depends in general on the directions of observation and illumination relative to the principal axes of the crystal. The angular variation of the scattering gives information about the symmetry of the lattice vibration responsible. The anisotropy of the scattering can be predicted for a vibration of any given symmetry by standard group-theoretical methods or by simple symmetry arguments not using group theory directly (Saksena 1940, Mathieu 1945, Ovander 1960).

The results of all the above authors, with several errors corrected, are collected together in table 1. Opposite each crystal class are listed the irreducible representations of the Raman-active lattice vibrations, using the notation of Herzberg (1945) and Wilson *et al.* (1955) for the irreducible representations (other authors sometimes have slightly different notations). Where an x , y or z occurs in brackets after an irreducible representation, this indicates that the vibration is also infra-red active and has the direction of polarization indicated. Such vibrations, which occur only in piezo-electric crystals (i.e. crystals with no centre of inversion symmetry) require a more detailed discussion and are treated in the following section. In crystals which do have a centre of inversion symmetry, only even-parity vibrations, whose representations have a subscript g , can be Raman active and only odd-parity (subscript u) vibrations can be infra-red active. This fact leads to the important complementary nature of infra-red absorption and Raman effect measurements. Directly above each irreducible representation is a matrix which gives the non-vanishing components of the Raman tensor, i.e. of $\alpha_{\rho\sigma,\mu}$ or $R_{\sigma\rho}^{\mu}$. The different elements of the matrices are the nine components of the tensor obtained by allowing both ρ and σ to take on the values x , y and z . Here x , y , and z are the crystal principal axes chosen to be identical with the principal axes x_1 , x_2 and x_3 defined for all the crystal classes by Nye (1957). The component μ of the phonon polarization for the case of infra-red-active vibrations is the quantity given in brackets after the irreducible representation symbol. For the unlisted case of triclinic symmetry, the Raman tensor is a general symmetric tensor.

As discussed in the previous section, the Raman tensor is strictly symmetric only when the phonon frequency is neglected in comparison with the radiation frequencies. Ovander (1960) has considered the form of the Raman tensor when this approximation is not made. In addition to the phonon symmetries listed in the table, other types of phonon are now Raman active and the scattering tensor contains in general an antisymmetric part. The additional Raman lines due to these other types of phonon should be very weak, and we shall assume the Raman tensor to be symmetric throughout the remainder of this article.

The table is used to calculate Raman scattering efficiencies as follows. Let the incident and scattered photons have polarizations in the directions of unit vectors \mathbf{e}_i and \mathbf{e}_s respectively. The scattering efficiency is given by:

Table 1. Raman-active vibrational symmetries and Raman tensors for the crystal symmetry classes.

System	Class	Raman tensors	
Monoclinic			
2	C_2	$\begin{pmatrix} a & d \\ b & c \end{pmatrix}$	$\begin{pmatrix} e & f \\ e & f \end{pmatrix}$
m	C_s	$A(y)$	$B(x, z)$
$2/m$	C_{2h}	$A'(x, z)$ A_g	$A''(y)$ B_g
Orthorhombic			
D_2	A	$\begin{pmatrix} a & & \\ & b & \\ & & c \end{pmatrix}$	$\begin{pmatrix} d & \\ & d \end{pmatrix}$
C_{2v}	$A_1(z)$		$\begin{pmatrix} e & \\ & e \end{pmatrix}$
D_{2h}	A_g		$\begin{pmatrix} B_3(x) \\ B_1(x) \\ B_{3g} \end{pmatrix}$
D_2	$A_1(z)$		$\begin{pmatrix} B_3(y) \\ B_1(x) \\ B_{3g} \end{pmatrix}$
C_{2v}	A	$\begin{pmatrix} a & & \\ & b & \\ & & c \end{pmatrix}$	$\begin{pmatrix} d & e \\ d & -c & f \\ e & f & e \end{pmatrix}$
C_{3v}	$A_1(z)$		$\begin{pmatrix} E(y) \\ E_g \end{pmatrix}$
$\bar{3}$	A_g		$\begin{pmatrix} E(x) \\ E_g \end{pmatrix}$
Trigonal			
C_3	A	$\begin{pmatrix} a & & \\ & a & \\ & & b \end{pmatrix}$	$\begin{pmatrix} c & d & e \\ d & -c & f \\ e & f & e \end{pmatrix}$
C_{3i}	A_g		$\begin{pmatrix} E(y) \\ E_g \end{pmatrix}$
C_3	A	$\begin{pmatrix} a & & \\ & a & \\ & & b \end{pmatrix}$	$\begin{pmatrix} -c & -d \\ -c & -d \end{pmatrix}$
C_{3i}	A_g		$\begin{pmatrix} E(y) \\ E_g \end{pmatrix}$
D_3	A_1		$\begin{pmatrix} E(y) \\ E(-x) \\ E_g \end{pmatrix}$
C_{3v}	$A_1(z)$		$\begin{pmatrix} E(x) \\ E(y) \\ E_g \end{pmatrix}$
$3m$	A_{1g}		$\begin{pmatrix} E(y) \\ E(-x) \\ E_g \end{pmatrix}$
Tetragonal			
C_4	A(z)	$\begin{pmatrix} a & & \\ & a & \\ & & b \end{pmatrix}$	$\begin{pmatrix} c & d \\ d & -c \end{pmatrix}$
S_4	A		$\begin{pmatrix} e & f \\ e & f \end{pmatrix}$
C_{4h}	A_g		$\begin{pmatrix} B \\ B(z) \\ B_g \end{pmatrix}$
C_4	A(z)		$\begin{pmatrix} E(x) \\ E(x) \\ E_g \end{pmatrix}$
S_4	A		$\begin{pmatrix} E(x) \\ E(x) \\ E_g \end{pmatrix}$
C_{4h}	A_g		$\begin{pmatrix} E(y) \\ E(-y) \\ E_g \end{pmatrix}$

	$\begin{pmatrix} a \\ a \\ b \end{pmatrix}$	$\begin{pmatrix} c \\ -c \end{pmatrix}$	$\begin{pmatrix} d \\ d \end{pmatrix}$	$\begin{pmatrix} e \\ e \end{pmatrix}$	$\begin{pmatrix} e \\ e \end{pmatrix}$
4mm	$A_1(z)$	B_1	B_2	$E(x)$	$E(y)$
422	A_1	B_1	B_2	$E(-y)$	$E(x)$
42m	A_1	B_1	$B_2(z)$	$E(y)$	$E(x)$
4/mmm	A_{1g}	B_{1g}	B_{2g}	E_g	E_g
	$\begin{pmatrix} a \\ a \\ b \end{pmatrix}$	$\begin{pmatrix} c \\ d \\ d \end{pmatrix}$	$\begin{pmatrix} -d \\ c \end{pmatrix}$	$\begin{pmatrix} e \\ f \\ -e \end{pmatrix}$	$\begin{pmatrix} f \\ -e \\ -f \end{pmatrix}$
6	$A_1(z)$	$E_1(x)$	$E_1(y)$	E_2	E_2
$\bar{6}$	A'_1	E''_1	E''_1	$E'(x)$	$E'(y)$
6/m	A_g	E_{1g}	E_{1g}	E_{2g}	E_{2g}
	$\begin{pmatrix} a \\ a \\ b \end{pmatrix}$	$\begin{pmatrix} c \\ c \end{pmatrix}$	$\begin{pmatrix} -c \\ -c \end{pmatrix}$	$\begin{pmatrix} d \\ d \end{pmatrix}$	$\begin{pmatrix} d \\ -d \end{pmatrix}$
622	A_1	$E_1(x)$	$E_1(y)$	E_2	E_2
6mm	$A_1(z)$	$E_1(y)$	$E_1(-x)$	E_2	E_2
6m2	A_1	E''_1	E''_1	$E'(x)$	$E'(y)$
6/mmm	A_{1g}	E_{1g}	E_{1g}	E_{2g}	E_{2g}
	$\begin{pmatrix} a \\ a \\ b \end{pmatrix}$	$\begin{pmatrix} b \\ b \\ b \end{pmatrix}$	$\begin{pmatrix} b \\ b \\ b \end{pmatrix}$	$\begin{pmatrix} d \\ d \end{pmatrix}$	$\begin{pmatrix} d \\ d \end{pmatrix}$
23	A	E	E	$F(x)$	$F(z)$
m3	A_g	E_g	E_g	F_g	F_g
432	A_1	E	E	F_2	F_2
43m	A_1	E	E	$F_2(x)$	$F_2(z)$
m3m	A_{1g}	E_g	E_g	F_{2g}	F_{2g}

$$S = A \left[\sum_{\rho, \sigma = x, y, z} e_1^\sigma R_{\sigma\rho} e_s^\rho \right]^2, \quad (36)$$

where A is a constant of proportionality and e_1^σ and e_s^ρ are components of the unit vectors along the principal axes σ and ρ . For two- or three-fold degenerate phonons the contributions of the two or three matrices given in the table are added to find the total scattering efficiency. As examples of the use of the tables, we consider the scattering geometry shown in figure 5. For the B phonon symmetry in the C_4 group, the Raman efficiency for scattered light polarized in the plane of scattering (i.e. the xz -plane) is:

$$S_{\parallel} = A(e_1^x c + e_1^y d)^2 \cos^2 \psi \quad (37)$$

and for scattered light polarized perpendicular to the plane of scattering is:

$$S = A(e_1^x d - e_1^y c)^2, \quad (38)$$

where the scattered light has been assumed to be approximately transverse even for the extraordinary ray. For the F_{2g} vibration in the O_h group, the analogous quantities are:

$$S_{\parallel} = Ad^2[(e_1^x \sin \psi)^2 + (e_1^y)^2], \quad (39)$$

$$S_{\perp} = Ad^2(e_1^x)^2. \quad (40)$$

When $\psi = \pi/2$ the sum of S_{\parallel} and S_{\perp} contains three terms which are the same three as occur in (31).

Experimentally it is more common to keep the directions of incident and scattered light fixed at right-angles to each other and to vary the orientation of the crystal axes relative to the light directions. A special case of this geometry is shown in figure 6. As an example, consider a phonon of A_1 symmetry in the group D_4 or D_6 . The scattering efficiencies are:

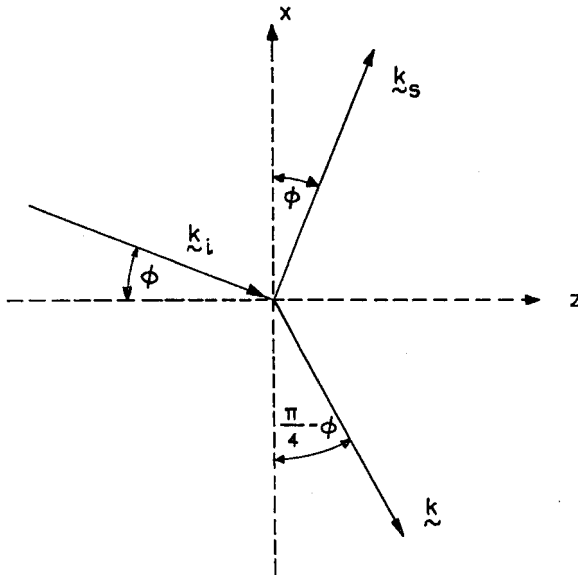


Figure 6. Alternative Raman scattering geometry.

$$S_{\parallel} = A[e_1^x a \sin \phi - e_1^z b \cos \phi]^2 = A(e_1^{\parallel})^2 \frac{1}{4}(a-b)^2 \sin^2 2\phi, \quad (41)$$

$$S_{\perp} = A(e_1^y a)^2 = A(e_1^{\perp} a)^2, \quad (42)$$

where e_1^{\parallel} and e_1^{\perp} are the components of \mathbf{e}_1 parallel and perpendicular to the plane of scattering (the light waves are assumed transverse). These last equations have been derived and discussed by Poulet (1955).

An important quantity, usually defined for scattering through a right-angle as in figure 6, is the depolarization ratio ρ . This is defined to be the ratio of the intensity of the component of scattered radiation polarized parallel to the plane of scattering to the intensity of the component polarized perpendicular to the scattering plane. Expressed in terms of scattering efficiencies:

$$\rho = \frac{S_{\parallel}}{S_{\perp}}. \quad (43)$$

The depolarization ρ evidently depends on the angle ϕ , and its magnitude and angular variation provide important information for deciding the symmetry type of an observed Raman line. Only the A and E symmetry vibrations in cubic crystals produce scattered light with a depolarization ratio ρ independent of ϕ . Saksena (1940) has tabulated theoretical depolarization ratios for many crystal symmetries and for three different states of polarization of the incident light; he considers both forward (longitudinal) and right-angle (transverse) scattering. Whereas Saksena's, results are restricted to light propagated along principal axes, Chandrasekharan (1963) has calculated the Raman scattering matrix for cubic crystals for any arbitrary relative orientations of crystal axes, incident-light wave vector and scattered-light wave vector.

Finally, we mention that Theimer (1955, 1956) in attempting to remove difficulties in the interpretation of measured intensities and depolarization ratios in calcite, has proposed that in some cases the appropriate symmetry group to use is not that of the crystal lattice but only its sub-group of operations which leave the phonon wave vector \mathbf{k} invariant. We feel that the validity of this approach has not been established.

2.4. Extensions of the theory for piezo-electric crystals

The theories reviewed so far provide an adequate basis for interpreting the first-order Raman spectra produced by scattering from non-polar lattice vibrations. However, extensions of the theory are necessary to deal with scattering from lattice vibrations which are simultaneously Raman and infra-red active. Experimentally, this type of scattering was regarded as anomalous, until its features were explained theoretically by Poulet (1955). The scattering is 'anomalous' in two ways:

(1) More first-order Raman peaks are observed than would be expected on the basis of a group-theoretical treatment of the symmetries of the vibrations. This is due to a lifting of the group-theoretical degeneracy of polar lattice vibrations by long-range electrostatic forces as discussed in §2.1 and illustrated in figs. 1, 2 and 3. In these figures, the group-theoretical degeneracy is that existing at $k=0$, while the phonon frequencies observed in the Raman effect are those at the right-hand edges of the figures. In uniaxial crystals, some of the Raman frequencies show an angular dependence. All these features have been fully discussed in §2.1.

(2) The experimental magnitudes and angular dependencies of the scattering efficiencies and depolarization ratios are not in agreement with the theoretical expressions given in §§2.2 and 2.3, even when the lifting of group-theoretical degeneracies is taken into account. This is again due to the long-range electric fields associated with the polar vibrations. The electric fields give rise to an electron-lattice interaction additional to the deformation potential type, and this interaction varies with phonon direction due to the variation in field strength.

In this section we review the theory of these anomalies. It is convenient to divide the discussion into two parts, for cubic and uniaxial crystals.

(i) *Cubic crystals.* As discussed in §2.1.1, the threefold Raman and infra-red-active vibration in a cubic crystal splits into two vibrations, one transversely and the other longitudinally polarized. Consider, for example, the F_2 vibration in a crystal of T_d symmetry, a case treated by Poulet (1955). In the previous section we have calculated the scattering efficiencies from the analogous vibration in a crystal with inversion symmetry (F_{2g} in O_h) using the basic equation (36). According to this equation the scattering efficiency is obtained by adding the contributions of the three matrices given in the table. However, when the threefold degeneracy is lifted it is necessary to take account of the fact that the three matrices correspond to polarization components of the phonon along the three principal axes, and these components can no longer all be chosen to be unity. It is thus necessary to generalize (36) by introducing a unit vector ξ in the direction of the mechanical polarization of the phonon. The formula for the scattering efficiency then becomes:

$$S = A \left[\sum_{\rho, \sigma, \tau = x, y, z} e_i^\sigma R_{\sigma\rho}^\tau \xi^\tau e_s^\rho \right]^2, \quad (44)$$

where τ is given in brackets in the table after the appropriate irreducible representation symbols. The contributions of the three matrices in the table for a phonon of given polarization are now summed before taking the square in (44).

For a threefold degenerate vibration like F_{2g} in O_h , (44) gives a result identical to that given by (36). However, for the F_2 vibration of T_d , assuming the scattering geometry of figure 5, the longitudinal vibration gives scattering efficiencies:

$$S_{\parallel}^l = A' d^2 (e_1^y \sin 3\psi/2)^2, \quad (45)$$

$$S_{\perp}^l = A' d^2 (e_1^x \sin \psi/2)^2. \quad (46)$$

For the transverse vibration, the contributions to the scattering by phonons polarized parallel and perpendicular to the scattering plane add to give:

$$S_{\parallel}^t = A d^2 [(e_1^y \cos 3\psi/2)^2 + (e_1^x \sin \psi)^2], \quad (47)$$

$$S_{\perp}^t = A d^2 (e_1^x \cos \psi/2)^2. \quad (48)$$

Note that $S_{\parallel}^l + S_{\parallel}^t = S_{\parallel}$ given by (39) and $S_{\perp}^l + S_{\perp}^t = S_{\perp}$ given by (40) provided that $A = A'$. Results equivalent to (45) to (48) have been given by Ovander (1962a), who calculated the form of the Raman tensor for this case by direct expansion of the electronic wave-functions in a power series in the phonon displacement coordinates, as is done in the Born theory of Raman scattering by non-polar lattice vibrations. Ovander has drawn attention to the fact that the scattering efficiencies for the transverse and longitudinal phonons are not symmetrical about $\psi = \pi/2$, in contrast

to the scattering efficiency for the threefold degenerate vibration; the transverse vibration gives greater scattering in forward directions, and the longitudinal vibration in backward directions. Poulet (1955) has given formulae for the intensities and depolarization ratios of light Raman scattered through a right-angle by cubic crystals having various orientations with respect to the light beams.

The constant of proportionality for scattering by the longitudinal vibration in (45) and (46) has been distinguished by a prime from the constant occurring in (47) and (48) for scattering by the transverse vibration. That the two constants should be different was first noted experimentally by Couture-Mathieu and Mathieu (1953) and the phenomenon was subsequently explained theoretically by Poulet (1955). It is due to the fact that the electric field accompanying a polar lattice vibration provides an additional electron–lattice interaction mechanism. This mechanism is well known in the realm of electron transport theory in the group III–V semiconductors, where it is known in some cases to lead to a stronger electron–phonon coupling than the deformation potential interaction (Ehrenreich 1957). In making a calculation of the Raman scattering produced by this additional mechanism, it is necessary to decide whether the electrons in the crystal experience the macroscopic field \mathbf{E}_{mac} or the local field $\mathbf{E}_{\text{local}}$ produced by the polar phonon. The two fields are related by:

$$\mathbf{E}_{\text{local}} = \mathbf{E}_{\text{mac}} + \frac{4\pi}{3} \mathbf{P}, \quad (49)$$

where \mathbf{P} is the polarization. It has been shown in §2.1 that the transverse phonon has $\mathbf{E}_{\text{mac}} = 0$, while the longitudinal phonon has \mathbf{E}_{mac} given by (6). Thus if the electrons of importance in the Raman effect experience \mathbf{E}_{mac} , the additional scattering mechanism occurs only for the longitudinal phonons. This is the point of view adopted by Ovander (1962a) and Loudon (1963b) and in the transport theory of polar semiconductors. However, Poulet (1955) assumes that the electrons experience $\mathbf{E}_{\text{local}}$, which leads to additional scattering for both transverse and longitudinal phonons. The calculations of Darwin (1934) and Nozières and Pines (1958) show that \mathbf{E}_{mac} should be used in crystals where the electrons are not localized on individual atoms (e.g. semiconductors), whereas $\mathbf{E}_{\text{local}}$ should be used for crystals where the electrons are tightly bound to the atoms.

Explicit calculations of the Raman scattering produced by the polar interaction have been fully carried out only for the phonons in the zinc blende lattice. There are two methods of calculation corresponding to the two methods of obtaining the non-polar scattering efficiency described in §2.2. Poulet (1955) has extended the Born and Bradburn method by expanding the polarizability $\alpha_{\rho\sigma}$ in a power series similar to (23), but with terms in the phonon electric field included, in addition to the terms in the phonon displacement \mathbf{r} . For cubic crystals both the phonon displacement and electric field point in the same direction, so that the symmetries of the scattering produced by the two electron–lattice interactions are identical. In the expansion of $\alpha_{\rho\sigma}$, the term linear in the electric field has as its coefficient the rate of change of polarizability with applied electric field. This quantity can be related to the linear electro-optic coefficients of the crystal (see Nye 1957), for the change in the component $\epsilon_{\mu\nu}$ of the optical dielectric constant tensor ϵ produced by an electric field \mathbf{E} is:

$$\delta\epsilon_{\mu\nu} = - \sum_{\rho,\sigma} \sum_{\tau} \epsilon_{\mu\rho} z_{\rho\sigma,\tau} \epsilon_{\sigma\nu} E_{\tau}, \quad (50)$$

where $z_{\rho\sigma\tau}$ is an electro-optic coefficient. The calculation thus leads to an expression for the polar Raman scattering which depends only on quantities which can be measured by independent experiments.

A similar result has been derived by Loudon (1963b), who calculated the scattering efficiency by third-order perturbation theory using (30) but with H_{EL} representing now the polar electron–lattice interaction. The scattered amplitude can be related to a microscopic expression for the electro-optic coefficients if the phonon frequency is negligible in comparison to the light frequencies. For a zinc blende type lattice, assuming the scattering geometry of figure 5 with $\psi = \pi/2$, and taking the case where the electrons experience \mathbf{E}_{mac} , the scattering efficiency for the transverse vibration using unpolarized incident light is obtained from (31), (47) and (48):

$$S_t = \frac{e^4 V (n_0 + 1) L d \Omega}{2 \hbar^3 m^4 d^2 M c^4 \omega_0} |R_{xy}^z|^2, \quad (51)$$

where the difference between the incident and scattered light frequencies has been ignored. For the longitudinal vibration, the calculation of Loudon gives a total scattering efficiency:

$$S_l = \frac{\hbar \omega_l (n_l + 1) L d \Omega}{4 \pi c^4} \left| \frac{e^2}{\hbar^2 \omega_l m^2 d} \left(\frac{\pi V}{M} \right)^{1/2} R_{xy}^z - \frac{\omega_l^2 \epsilon^2}{2} \left(\frac{2}{\epsilon} - \frac{1}{\epsilon^0} \right)^{1/2} z_{41} \right|^2, \quad (52)$$

where n_l is the Bose–Einstein factor for the longitudinal phonons of frequency ω_l , and z_{41} is the electro-optic coefficient for the zinc blende lattice in condensed notation (see Nye 1957). The calculation of Poulet (1955) using \mathbf{E}_{local} gives a result in which both S_t and S_l contain a term in z_{41} . Since R_{xy}^z is the only factor in (51) and (52) which cannot be otherwise measured, it should in principle be possible to determine which electric field acts on the electrons by measuring the relative intensities of the two Raman peaks and the incident light. Such an experiment would however be difficult in practice and there is little or no information in the literature on the relative intensities of incident and scattered radiation.

A different approach to the calculation of Raman scattering intensities has been followed by Ovander (1962b) and the method has been applied to cubic crystals by Grechko and Ovander (1962). In this method the crystal is regarded as a collection of interacting molecules and that part of the interaction between the radiation and the molecules which mixes the molecular electronic excited states with the ground state is diagonalized. The resulting eigenstates are mixtures of radiative and electronic excitations (polaritons). Ovander now considers three terms in the Hamiltonian which can cause Raman scattering from molecular vibrational levels. The part of the electron–radiation interaction which mixes two molecular excited states together is denoted H_A and gives a Raman scattering equivalent to that of §2.2 when the deformation potential electron–lattice interaction is inserted. The term arising from the $e^2 A^2 / 2mc^2$ part of the electron–radiation interaction (denoted H_B) leads to significant Raman scattering only for incident radiation in the x-ray region (see Peierls 1955 for a discussion of this type of scattering), and it is neglected by Ovander. Finally the intermolecular interaction term leads to a Raman scattering Hamiltonian H_C (called H_B in Ovander's later papers); when H_C arises from the interactions of the electronic and vibrational dipole moments of all the molecules in the crystal, the Hamiltonian produces the part of the Raman scattering due to the polar electron–lattice interaction already discussed in this section. Grechko and

Ovander (1962) show that this method of calculation leads to the expressions for the angular dependence of the scattering already given.

When the frequency ω_i of the incident light approaches one of the electronic excitation frequencies of the crystal, terms in the Raman tensor diverge, as is evident from (32). Ovander (1962b,c) has discussed this so-called resonance Raman scattering in terms of his theory outlined above. The divergence is removed by a proper consideration of the electron-radiation interaction in the region of the resonance. Loudon (1963b) has treated resonance scattering for a situation where ω_i is close to the forbidden energy gap frequency in an insulator. The Raman tensor is always finite in this case even using (32) without modification, due to the arrangement of the electronic energy levels in bands.

(ii) *Uniaxial crystals.* As discussed in § 2.1.2, a polar uniaxial crystal having two atoms in the unit cell may have three infra-red-active lattice vibration branches, two of the branches being degenerate for propagation parallel to the c -axis, one of these and the remaining branch having a frequency which depends on the direction of propagation. The angular dependence of the Raman scattering efficiencies can be calculated using the results of § 2.3 modified to take the effect of the long-range electric forces into account.

Let us consider the example of a crystal having C_{4v} symmetry. Reference to the table shows that group theoretically an infra-red and Raman-active phonon can be non-degenerate of type A_1 corresponding to lattice displacements parallel to the c -axis or twofold degenerate of type E corresponding to lattice displacements perpendicular to the c -axis. The long-range electric forces lift the twofold degeneracy and mix the A_1 and E symmetry phonons, so that for a general direction of propagation there are three non-degenerate types of phonon; two of which have neither purely A_1 nor purely E symmetry. Thus all three A_1 and E matrices contribute in general to the Raman scattering efficiency for two of the three phonon branches.

In addition to this feature, the formula (44) for the scattering efficiency must be further generalized to take account of the two types of electron-lattice interaction. In uniaxial crystals the lattice displacement \mathbf{r} (parallel to ξ), which controls the deformation potential scattering, is not in general parallel to the electric field \mathbf{E} (parallel to \mathbf{k}), which controls the polar scattering. Following the calculation of Poulet (1955), described in part (i) of this section, in which the Born and Bradburn method is extended by inclusion of terms in both \mathbf{r} and \mathbf{E} in the expansion of the polarizability $\alpha_{\rho\sigma}$, it is seen that (44) must be generalized to:

$$S = \left\{ \sum_{\rho, \sigma, \tau = x, y, z} e_i^\sigma R_{\sigma\rho}^T (\alpha \xi^\tau + \beta \hat{\mathbf{k}}^\tau) e_s^\rho \right\}^2, \quad (53)$$

where β is proportional to the electric field strength $|\mathbf{E}|$. The contributions of the three matrices in the table corresponding to polarization components in the x , y and z directions must be summed before taking the square in (53) (for symmetry groups D_3 , D_4 , C_{3h} , D_6 and D_{3h} there are only two matrices in the table, corresponding to polarization components in the x and y directions). We may note that (53) contains (44) as a special case. For cubic crystals, where ξ and $\hat{\mathbf{k}}$ point in the same direction for longitudinal vibrations, the constant of proportionality is $(\alpha + \beta)^2$, equal to A' in (45) and (46); for transverse vibrations, where β is zero, the constant of proportion-

ality is α^2 , equal to A in (47) and (48). In both cubic and uniaxial crystals β is always zero for exactly transverse branches.

Consider first a crystal of the type discussed in part (i) of §2.1.2 (electrostatic forces predominant over anisotropy in the short-range interatomic forces). These crystals have a quasi-longitudinal extraordinary phonon for which the almost constant electric field \mathbf{E} and the atomic displacement \mathbf{r} are approximately collinear. Assuming the geometry of figure 5, and taking the scattered light to be approximately transverse, the scattering efficiencies for this phonon for a crystal of C_{4v} symmetry are:

$$S_{\parallel} = \{e_1^x a \sin \psi/2 \cos \psi + e_1^x e \cos \psi/2 \sin \psi\}^2 (\alpha + \beta)^2, \quad (54)$$

$$S_{\perp} = \{e_1^y a \sin \psi/2\}^2 (\alpha + \beta)^2. \quad (55)$$

The quasi-transverse extraordinary phonon has negligible electric field, leading to:

$$S_{\parallel} = \{e_1^x a \cos \psi/2 \cos \psi - e_1^x e \sin \psi/2 \sin \psi\}^2 \alpha^2, \quad (56)$$

$$S_{\perp} = \{e_1^y a \cos \psi/2\}^2 \alpha^2, \quad (57)$$

while the transverse ordinary phonon finally gives:

$$S_{\parallel} = \{e_1^y e \sin \psi\}^2 \alpha^2, \quad (58)$$

$$S_{\perp} = 0. \quad (59)$$

For polar uniaxial crystals of the type discussed in part (ii) of §2.1.2 (anisotropy of the short-range interatomic forces predominant over electrostatic forces), the calculation of the Raman scattering efficiency from phonons which are infra-red active is a little more complicated. For these vibrations, the two extraordinary phonons have a lattice displacement \mathbf{r} directed approximately parallel or perpendicular to the c -axis, while the electric field \mathbf{E} is parallel to \mathbf{k} , as in (20) and (21). In addition, these equations show that the electric field strength itself has a strong angular dependence. These features lead to different angular dependences for the contributions to the scattering resulting from the deformation potential and polar electron–lattice interactions. We again assume a crystal of C_{4v} symmetry with the scattering geometry of figure 5. Consider first the extraordinary phonon associated with lattice displacements parallel to the c -axis, whose frequency and electric field strength are given by (18) and (20), i.e. the upper branch of figure 3. The scattering efficiencies are:

$$S_{\parallel} = \{e_1^x a [\alpha + \beta \sin^2 \psi/2] \cos \psi + e_1^x e \beta \sin \psi/2 \cos \psi/2 \sin \psi\}^2, \quad (60)$$

$$S_{\perp} = \{e_1^y a [\alpha + \beta \sin^2 \psi/2]\}^2, \quad (61)$$

where the $\sin \psi/2$ dependence of β has been displayed explicitly. This result (with a $\cos \psi$ factor omitted) has been obtained by Ovander (1962d) using his method of calculation outlined above. The second extraordinary phonon has its lattice displacement approximately parallel to the x -axis; the frequency and electric field of this branch are given by eqns. (19) and (21). The scattering efficiencies are:

$$S_{\parallel} = \{e_1^x a \beta \cos \psi/2 \sin \psi/2 \cos \psi - e_1^x e [\alpha - \beta \cos^2 \psi/2] \sin \psi\}^2, \quad (62)$$

$$S_{\perp} = \{e_1^y a \beta \cos \psi/2 \sin \psi/2\}^2. \quad (63)$$

There is a small additional angular variation in these last four equations due to the dependence of the phonon frequency on angle, since the equations for S contain this frequency as a factor (cf. the corresponding equations (51) and (52) for the cubic case). Finally, the scattering efficiencies for the ordinary phonon are the same as those given previously in (58) and (59). Ovander (1962d) has also given results for these last two branches.

Poulet (1955) has derived results for Raman scattering by the phonon whose lattice displacements are parallel to the c -axis, in the geometry of figure 6. Poulet uses again the local field of the lattice vibration, whereas the results of this section have assumed the macroscopic field to be the appropriate one. The latter assumption gives:

$$S_{\perp} = \{e_i^{\perp} a[\alpha + \beta \sin^2(\pi/4 - \phi)]\}^2, \quad (64)$$

while S_{\parallel} is rather complicated and will not be written down. In fact, Poulet's calculation refers to a C_{6v} symmetry crystal, but the appropriate tensors have the same symmetry. The corresponding non-polar A_1 vibration, in crystal of D_4 or D_6 symmetry, has already been treated in (41) and (42).

There have been no calculations of the constants of proportionality occurring in the equations for the scattering efficiency in uniaxial crystals, analogous to (51) and (52) for cubic crystals. It would not be difficult to make such a calculation for a specific crystal symmetry. The polar part of the scattering would again lead to terms proportional to electro-optic coefficients when the phonon frequency could be neglected in comparison with ω_i and ω_s .

2.5. Temperature effects

There have been several experimental studies of the dependence of Raman spectra on temperature. Both the Raman shifts and linewidths, and also the scattered intensities vary with temperature.

The variation with temperature of the shifts and widths of Raman lines has been measured in quartz by Nedungadi (1940), in diamond by Krishnan (1946a), in calcite and quartz by Narayanaswamy (1947), and in topaz by Srinivasan (1953). The common features are a broadening of the Raman lines with increase in temperature accompanied by a shift of the Stokes lines to higher frequencies. The amount of temperature shift is different for different Raman lines, being in general larger for the lines of higher frequency. That is, the phonon frequencies decrease with increasing temperature, the decrease being larger the smaller the phonon frequency.

These features can be qualitatively understood in terms of the anharmonic forces in the crystal lattice. The width and temperature shift of the Raman lines are the same as the phonon width and shift which are observed experimentally in other types of experiment, e.g. neutron scattering or infra-red absorption by phonons, and theoretical expressions for them can be derived quantum mechanically. Inclusion of anharmonic forces leads to the replacement of the total scattering efficiency S , given for example by (31), by a scattering efficiency $S(\omega_s) d\omega_s$ defined in terms of the fractional number of incident photons converted into scattered photons having their frequencies in a range $d\omega_s$ about ω_s . This efficiency can be shown to satisfy the relation:

$$S(\omega_s) = \frac{S}{\pi} \frac{\Gamma}{(\omega_i - \omega_0 - \omega_s - \Delta)^2 + \Gamma^2}. \quad (65)$$

The Raman scattered radiation thus has a Lorentzian distribution about the frequency $\omega_i - \omega_0 - \Delta$ with a half-width Γ . The total scattering efficiency is still the quantity S , since

$$\int S(\omega_s) d\omega_s = S. \quad (66)$$

Quantum-mechanical expressions for the shift Δ and half-width Γ due to third-order anharmonic forces have been given by Maradudin *et al.* (1962). Fourth-order anharmonic forces may also make significant contributions to Γ and Δ at high temperatures. The expressions for Γ and Δ are too complicated to be evaluated explicitly except for simplified lattice models. However, from the form of the expressions it is clear that the magnitudes of both Γ and Δ should increase with temperature, the dependence on temperature being linear when $k_B T/\hbar$ is much greater than the phonon frequencies. This agrees with the experimental results, which show a linear dependence of Γ and Δ on temperature at sufficiently high temperatures. In fact the change of phonon frequency with temperature is due not only to the anharmonic coupling of the Raman phonons to other vibrations, but also to the thermal expansion of the lattice (see Maradudin 1962 and Maradudin and Fein 1962). A complete discussion of Δ and its temperature variation must take this factor into account. Viswanathan (1963) has also derived expressions for the width and temperature shift of Raman lines; his results do not appear to agree with those of the authors cited above.

The theoretical scattered intensities and efficiencies also depend on temperature, by a factor $n_0 + 1$ for Stokes lines and a factor n_0 for anti-Stokes lines. There have been several experimental investigations of the temperature dependence of the intensities of Stokes lines. Bobovich and Tulub (1959, 1960) have investigated nine types of crystal, including quartz, calcite and CaF_2 , and these last three crystals have been subsequently re-studied by Stekhanov and Chisler (1962). Stekhanov (1955) has measured temperature-dependent intensities in gypsum. The experiments require care and some of the earlier measurements produced spurious results (see the criticism of earlier work in Stekhanov and Chisler 1962). The lines studied have an intensity which either increases at the theoretical rate or increases more slowly than predicted, except for one of the Raman lines in quartz which appears to increase more rapidly than the theory predicts. The falling of the intensity below that expected theoretically in some cases is not entirely understood. Some of the loss as the sample is heated may be due to the increasing breadth of the Raman lines which causes a progressively larger fraction of the line intensity to move out into the wings of the line and escape detection. Theimer (1956) has suggested that departures of the temperature dependence from the theoretical $(n_0 + 1)$ factor may be due to more complicated Raman scattering processes in which an extra step involving the creation and destruction of a virtual phonon occurs. This type of process is made possible by the existence of third-order anharmonic forces in the lattice.

2.6. Experimental results

A list of experimental work is given in a separate group of references at the end of the article. The list is not completely exhaustive and references to some of the work on more complex crystals (e.g. sulphates and hydroxides) has been omitted. In much of this work only a few of the Raman-active vibrations are observed and no

interpretation of the measurements is possible. Of the work which is listed some of the more interesting measurements are singled out here for discussion.

2.6.1. Piezo-electric crystals

Mathieu and his collaborators have published a series of papers containing the results of measurements on piezo-electric crystals, and the theoretical work of Poulet (1955) reviewed in § 2.4 is based upon some of the earlier measurements in the series. Couture-Mathieu, Poulet and Mathieu (1952) have measured the Raman spectra of NaClO_3 and NaBrO_3 . These crystals belong to the cubic symmetry group T, and the longitudinal and transverse vibrations of type F exhibit values of the depolarization ratio which can be quite well accounted for by the theory of Poulet, but which were thought to be anomalous before the important theoretical modifications required for piezo-electric crystals were fully understood. A similarly good agreement with theory is obtained for the case of ZnS in the zinc blende structure (Couture-Mathieu and Mathieu 1953). The lattice has T_d symmetry with single transverse and longitudinal optic vibrations of F_2 symmetry, whose measured frequencies (274 cm^{-1} and 349 cm^{-1} respectively) are in good agreement with the Lyddane-Sachs-Teller relation (Poulet 1954, 1955). Recent measurements on CuCl (Mathieu *et al.* 1960), which has the same structure, have only resolved a single Raman line, presumably that of the longitudinal optic branch which in the case of zinc blende is ten times more intense than the line due to the transverse optic branch. Thus in both ZnS and CuCl the scattering produced by the polar electron-lattice interaction appears to dominate that produced by the deformation potential interaction.

For the case of uniaxial crystals, the theory of § 2.4 has been compared with the Raman spectrum of lithium perchlorate hydrate measured by Mathieu and Couture-Mathieu (1952a). The crystal has symmetry class C_{6v} , and the vibrations of symmetries A_1 and E_1 are both Raman and infra-red active. One of the observed Raman peaks exhibits a frequency which depends on crystal orientation, following a relation similar to (18). This vibration has thus been assigned to the A_1 symmetry type by Poulet, who has also shown that the variation of Raman intensity with orientation may be represented by an equation similar to (64). One of the other Raman peaks also has a frequency variation which appears to follow (18).

Other measurements in the series by Mathieu and co-workers have detected angular dependencies of the Raman peaks which can be interpreted in terms of Poulet's theory for piezo-electric crystals (see Mathieu and Couture-Mathieu 1952b, Weil and Mathieu 1954, Mathieu *et al.* 1955, Poulet and Mathieu 1956). Haas and Hornig (1959) have collected together many of the values of transverse and longitudinal frequencies measured by Mathieu and his co-workers.

2.6.2. Quartz

In the period under review there have been more measurements of the Raman spectrum of quartz than of any other crystal. Quartz has a strong Raman spectrum with a number of well-resolved lines. The crystal symmetry group of α -quartz is D_3 and there are three SiO_2 groups in the unit cell leading to four A_1 and eight E vibrations which can contribute to the Raman spectrum. The remaining degrees of freedom are taken up by the three acoustic modes and four infra-red-active A_2 vibrations. The E vibrations are also infra-red active and the resulting angular dependencies of the frequencies and intensities of some of the E vibrations have been observed by Mathieu and Couture-Mathieu (1952b). A recent re-measurement of the

Raman spectrum of quartz has been made by Krishnamurti (1958). Zubov and Osipova (1961) have made careful measurements of the widths and shapes of 11 lines in the Raman spectrum of quartz at room temperature; they find that all the lines have a shape close to Lorentzian with widths ranging from 4 cm^{-1} to 21 cm^{-1} . The same authors (Zubov and Osipova 1962) have shown that neutron irradiation of α -quartz produces shifts and increased breadths of the Raman lines, and Zubov *et al.* (1962) have observed small intensity changes in two of the Raman lines when an electric field is applied to the crystal.

The infra-red lattice bands of α -quartz have been measured by Spitzer and Kleinman (1961) and the observed E vibrations have been compared with the same vibrations observed in Raman scattering. These same authors (Kleinman and Spitzer 1962) have made a theoretical study of the four A_1 and four A_2 optical vibrations, obtaining good agreement with experiment.

The Raman spectrum of vitreous silica has been measured by Krishnan (1953) and Flubacher *et al.* (1959). The two measurements give results which agree in their general features. The spectrum exhibits broad bands rather than sharp peaks and its most striking feature is an intense continuum which extends from shifts of 8 cm^{-1} to 560 cm^{-1} . The spectrum of vitreous silica is thus markedly different from that of α -quartz.

2.6.3. Alkaline-earth fluorides

These crystals have recently become important as host lattices for rare earth ions used in producing laser emission. The spectral lines due to electronic transitions of rare earth ions in crystals frequently exhibit side bands, due to transitions in which phonons are simultaneously created or destroyed, and the displacements of the side bands give information about the lattice vibration frequencies. The phonon-assisted transitions are known as vibronics. The fluorides have symmetry group O_h with one group of three atoms in the unit cell, leading to one Raman-active F_{2g} optic branch and one infra-red-active F_{1u} branch. Wood and Kaiser (1962) have measured the absorption and fluorescence spectra of Sm^{2+} in CaF_2 , SrF_2 and BaF_2 . For SrF_2 they find that one of the vibronic side bands has a shift of 282 cm^{-1} , which is close to the shift of 280 cm^{-1} of the single strong line in the Raman spectrum of SrF_2 measured by Richman (1964). For BaF_2 , the corresponding vibronic shift is 244 cm^{-1} , which compares with the Raman shift measured by Krishnan and Narayanan (1963) to be 244 cm^{-1} and by Richman (1964) to be 243 cm^{-1} . For CaF_2 the Raman shift observed by Ananthanarayana (1962) is 322 cm^{-1} , but Wood and Kaiser do not see any vibronic shift close to this frequency.

Mention may also be made of the measurements of Richman *et al.* (1963), who have correlated the Raman spectrum of LaCl_3 with the vibronic transitions of Pr^{3+} in LaCl_3 .

2.6.4. Wurtzite structure crystals

The wurtzite lattice has C_{6v} symmetry and is one of the simplest structures of uniaxial crystal, being obtained from the cubic zinc blende (T_d) lattice by a rearrangement of the planes of atoms perpendicular to the (111) axis (Birman 1959). There are four atoms in the unit cell, leading to single A_1 and E_1 optic branches which are both Raman and infra-red active, two E_2 branches which are Raman active, and two inactive B branches in addition to the A_1 and E_1 acoustic branches. The Raman spectra of SiC and ZnS having the wurtzite structure have

been measured. Both these crystals occur also in cubic T_d symmetry modifications, and individual atoms have the same nearest neighbour configuration in both structures leading to some similarities in the phonon spectra. Merten (1962) has discussed the modifications in the phonon spectra on changing from a zinc blende to a wurtzite lattice in terms of a halving of the Brillouin zone dimension in the (111) direction. The main effect of the transition is then a folding back of the phonon branches at the new zone boundary, frequencies which previously occurred at the symmetry point L in the zinc blende Brillouin zone now occurring at the centre of the wurtzite Brillouin zone. The anisotropy in the interatomic forces for these wurtzite structure crystals is very small, and the discussion of §2.1.2, part (i) applies, the angular dependence of the phonon frequencies being small, as illustrated in figure 2.

The Raman spectrum of SiC has been measured by Mathieu and Poulet (1957), but the interpretation which they give must be modified in the light of a subsequent measurement of the infra-red properties of SiC by Spitzer, Kleinman and Walsh (1959). The Raman measurements were made with incident light directed parallel to the c -axis and scattered light viewed at right angles. The line observed at 797 cm^{-1} is close to the ordinary absorption resonance frequency observed by Spitzer *et al.* and must have E_1 symmetry. The Raman lines observed at 789 cm^{-1} and $966\text{--}969\text{ cm}^{-1}$ (the doublet nature of this line is not accounted for) are evidently due to the transverse-like and longitudinal-like phonons of intermediate $A_1\text{--}E_1$ symmetry. The former frequency is close to the extraordinary ray resonance frequency observed by Spitzer *et al.* (for light propagated perpendicular to the c -axis) and the latter frequency is close to that predicted by the Lyddane–Sachs–Teller relation. For SiC accordingly, ω_{\parallel} is smaller than ω_{\perp} , opposite to the relative values assumed for figure 2. The remaining Raman lines at 335 cm^{-1} and 764 cm^{-1} can now be assigned to the two E_2 phonons. Spitzer, Kleinman and Frosch (1959) have measured the ordinary ray resonance frequency in *cubic* SiC and find it to be equal to the corresponding frequency in the *hexagonal* (wurtzite) form of SiC.

Mathieu *et al.* (1963) have measured the Raman spectrum of ZnS in the wurtzite structure. They observed three of the first-order Raman-active phonons, two of the observed frequencies being equal to the frequencies of the transverse and longitudinal optic phonons in cubic ZnS, and thus of $A_1\text{--}E_1$ symmetry. The remaining peak at 217 cm^{-1} is evidently due to a phonon of E_2 symmetry.

2.6.5. Ferro-electric crystals

The Raman spectra of several ferro-electric crystals have been measured. Such crystals are particularly interesting for Raman measurements because the lattice symmetry changes when the crystal is cooled through its transition temperature, leading to corresponding changes in the spectra. Thus in Rochelle salt, Stekhanov and Gabrichidze (1963) have observed changes in Raman shifts and intensities when the crystal passes from its D_{2d} para-electric state to its C_2 symmetry ferro-electric state, although the complexity of the crystal structure prevents a complete interpretation of the observed effects. In crystals of C_2 symmetry, all vibrations are Raman active while in D_{2d} symmetry all except one of the five vibrational symmetries are Raman active, so that no great change in the selection rules occurs between the para- and ferro-electric phases.

For the barium titanate structure however, the para-electric crystal symmetry is O_h with the five atoms in the unit cell all situated at centres of inversion, leading to four Raman-*inactive* optic modes, three of F_{1u} symmetry and one of F_{2u} symmetry.

In the highest temperature ferro-electric phase the symmetry reduces to C_{4v} and the optic vibrations become first-order Raman-active, three of A_1 symmetry, one of B_1 symmetry and four of E symmetry. Barium titanate itself ($BaTiO_3$) has a transition temperature of $120^\circ C$ and Bobovich and Bursian (1961) have measured its Raman spectrum in the ferro-electric tetragonal phase at room temperature. Only three Raman lines are observed and a complete interpretation is not possible. Bobovich and Bursian discuss the spectrum in terms of the normal vibrations of a Ti ion and its six O nearest neighbours. Ikegami (1964) has recently observed a larger number of lines in the Raman spectrum of $BaTiO_3$. The agreement between these two measurements is not very good. The Raman spectrum of strontium titanate ($SrTiO_3$) at room temperature has been measured by Narayanan and Vedam (1961). Strontium titanate may have a ferro-electric transition in the region of $35^\circ K$, but at room temperature it is para-electric with cubic O_h symmetry and is not expected to exhibit a first-order Raman spectrum. The peaks observed by Narayanan and Vedam must therefore be a second-order Raman spectrum, although the authors try to interpret their results as a first-order spectrum.

Of much greater value than either of the above experiments on the titanates would be a series of measurements of the Raman spectra at various temperatures above and below the transition temperature. The way in which a first-order Raman spectrum appears at the transition temperature could be determined and the variation of its intensity with temperature in the ferro-electric region would give an indication of the way in which the distortion of the lattice from its cubic structure varies with temperature. Above the transition temperature some of the low-frequency vibrations have a strongly temperature-dependent frequency (Cowley 1962) which could perhaps be investigated by the second-order Raman effect.

An attempt to observe effects of this type in NH_4HSO_4 and four other ferro-electrics has recently been made by Bazhulin *et al.* (1964). They measured Raman spectra at room temperature, and at lower temperatures in the regions of the ferro-electric transitions, but were unable to detect any low-frequency vibrations having markedly temperature-dependent frequencies.

2.6.6. Rutile

Titanium dioxide in the rutile structure is a fairly simple type of uniaxial crystal, having symmetry D_{4h} with two TiO_2 groups in the unit cell. The vibrational symmetries have been calculated by Dayal (1950), who finds that there are four Raman-active phonons, one each of symmetries A_{1g} , B_{1g} , B_{2g} and E_g .

The Raman spectrum of rutile has been investigated by Narayanan (1953) and Krishnamurti (1962). The latter author has assigned the four Raman-active phonon symmetries to four of the measured peaks, and has interpreted the remaining peaks as a second-order spectrum. This interpretation does not, however, seem to be altogether firmly established.

2.7. Brillouin scattering

2.7.1. Theory

All the previous discussion has been concerned with Raman scattering from optic vibrations of the lattice. Acoustic lattice vibrations can also give rise to first-order Raman scattering. This effect was predicted by Brillouin (1922) and is sometimes referred to as Brillouin scattering. Consider the scattering arrangement shown in figure 5, where \mathbf{k} now refers to the wave vector of an acoustic phonon. For the

Stokes component of the scattering the fractional shift in the frequency of the light is:

$$\frac{\omega_i - \omega_s}{\omega_i} = \frac{2\epsilon^{1/2}v}{c} \sin \frac{\psi}{2}, \quad (67)$$

using (28) and energy conservation. Here v is the velocity of the acoustic phonon, i.e. the appropriate sound velocity. For the anti-Stokes component the sign of the right-hand side is reversed. Since v/c is typically of order 10^{-5} , the Brillouin shifts are very small, of order 2 or 3 cm^{-1} for many crystals. There are three acoustic branches having different values of v for a general direction of propagation, leading to three Stokes and three anti-Stokes components in the Brillouin spectrum. The Stokes and anti-Stokes peaks for a given branch have almost equal intensity due to the smallness of the phonon frequency. The main value of measurements of the Brillouin spectra lies in the fact that the elastic constants of a crystal can be determined from a knowledge of the acoustic phonon velocities.

The theory of Brillouin scattering can be derived from a classical macroscopic standpoint, by considering the elastic deformation produced in a crystal by a long-wavelength acoustic phonon. A strain e_{ij} in the lattice produces a change in the component $\epsilon_{\mu\nu}$ of the optical dielectric constant tensor ϵ given by:

$$\delta\epsilon_{\mu\nu} = - \sum_{\rho,\sigma} \epsilon_{\mu\rho} p_{\rho\sigma,ij} \epsilon_{\sigma\nu} e_{ij}, \quad (68)$$

where $p_{\rho\sigma,ij}$ is an elasto-optical coefficient (Nye 1957). Thus an acoustic phonon of frequency ω produces a component of the dielectric constant oscillating with the same frequency, and an incident light wave of frequency ω_i causes polarization components in the lattice having frequencies $\omega_i \pm \omega$. This oscillating polarization re-radiates energy at the frequencies $\omega_s = \omega_i \pm \omega$ of the Brillouin components. The strain components e_{ij} associated with an acoustic vibration are readily calculated and expressions for Brillouin scattering efficiencies can be obtained in terms of quantities which can be independently determined. In some respects the calculation of scattering by acoustic phonons is similar to that for polar scattering by optic phonons in a piezo-electric crystal. In the former case the optical dielectric constant ϵ is modulated by a strain wave via the elasto-optic effect, while in the latter case ϵ is modulated by a long-wavelength electric wave via the electro-optic effect.

A good account of the macroscopic calculation of the Brillouin scattering is given by Born and Huang (1954). For scattering by a cubic crystal with unpolarized incident light and with incident and scattered light along four-fold axes at right angles to each other, the scattering efficiencies for the three acoustic phonons are:

$$S_1 = \frac{k_B T \omega_s^4 \epsilon^4 L d \Omega}{64 \pi^2 c^4} \left[\frac{p_{44}^2}{c_{44}} \right], \quad (69)$$

$$S_2 = 0, \quad (70)$$

$$S_3 = \frac{k_B T \omega_s^4 \epsilon^4 L d \Omega}{64 \pi^2 c^4} \left[\frac{2(p_{44}^2 + p_{12}^2)}{c_{11} + c_{12} + 2c_{44}} \right], \quad (71)$$

where p_{ij} and c_{ij} are the elasto-optic coefficients and elastic constants in condensed notation (Nye 1957). It has been assumed that $k_B T \gg \hbar\omega$, and the Stokes and anti-Stokes components then have the same intensity. Note that the subsequent

expressions given by Born and Huang on page 381 for scattering of polarized incident light by vibration 3 should be multiplied by a factor 2.

It is also possible to calculate the Brillouin scattering efficiencies using a microscopic model of the lattice. This has been attempted by Theimer (1951, 1952), who obtained results in disagreement with the above due to an error in his calculation (see the comments on p. 374 of Born and Huang 1954). The Brillouin scattering can also be calculated using a model in which the electron–lattice interaction is treated in the deformation potential approximation. This approach has been adopted by Loudon (1963b) and the calculation is exactly analogous to that for Raman scattering by optic phonons outlined in §§ 2.2 and 2.4. The scattering tensor in the acoustic phonon case can be related to the elasto-optic coefficients when the difference between ω_s and ω_i is ignored, and the final results of the calculation are in exact agreement with those of Born and Huang given in (69) to (71) above.

2.7.2. Experiment

Measurements of Brillouin spectra have generally been used to check already-known elastic constants rather than to obtain values of constants not previously known. An accuracy of about 1% can be achieved in Brillouin spectra measurements under favourable conditions. The first observation of this type of spectrum was made by Gross (1930) on quartz. Among subsequent measurements we may mention those of Krishnan on diamond (1947a,b), fused quartz (1953) and LiF, NaCl, KCl, diamond, α -quartz, calcite (CaCO_3), alumina (Al_2O_3) and barite ($\text{BaO} \cdot \text{SO}_2$) (1955). The results of these measurements for the acoustic phonon velocities check reasonably well with values determined from the known elastic constants. Fused quartz, being an isotropic substance, possesses only two acoustic phonon velocities, for longitudinal and transverse sound waves, and should have two Brillouin peaks on either side of the exciting line. Only the longitudinal peak was detected by Krishnan (1953), but Flubacher *et al.* (1959) have also observed the much weaker transverse peak. Geiger and Kulp (1960) have reported a failure to observe Brillouin scattering in three types of quartz glass.

3. Second-order Raman effect

3.1. Theory of the scattering process

The first-order Raman effect is a scattering process in which a single phonon is either created or destroyed. In the second-order Raman effect, two phonons participate in the scattering process. They may both be created (giving a Stokes component in the scattered light) or one may be created and the other destroyed (giving a Stokes or anti-Stokes component) or finally both may be destroyed (giving an anti-Stokes component). There are two types of second-order Raman scattering and they give rise respectively to a line spectrum and a continuous spectrum.

The second-order line spectrum is due to processes in which light has suffered two successive first-order Raman scatterings. The process is illustrated in figure 7, using the same notation as figure 4. Figure 7 refers to the case in which the two phonons, having frequencies ω_0 and ω'_0 , are created. It is essential that first-order Raman scattering should be allowed for the two phonons individually, and the frequency shifts which occur in the second-order line spectrum are sums and differences of the shifts which occur in the first-order spectrum. It is not necessary for energy to be

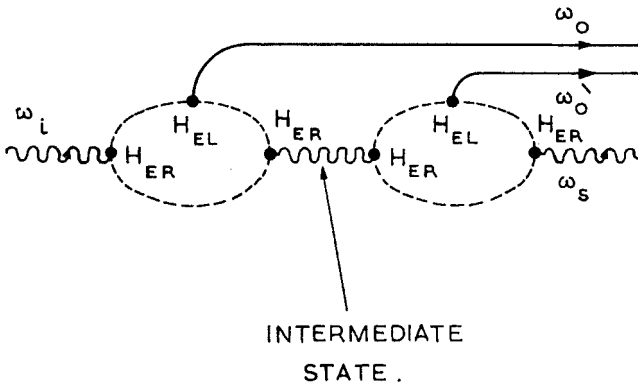


Figure 7. Elementary scattering process for the second-order line spectrum.

conserved in the intermediate state marked in figure 7. However, the total wave vector in this state must be the same as in the initial state and this conservation law forces the wave vector of the first phonon (ω_0) to be small and leads to the line nature of the resulting Raman spectrum. The second-order line spectrum provides no information about the phonon frequencies additional to that provided by the first-order spectrum, and we defer any further discussion to §3.3.1, where an estimate is made of the relative intensities of the first and second-order Stokes lines in diamond. Since the process depends on two successive scattering events, which must both take place within the crystal volume, the scattering efficiency for the second-order line spectrum increases with the size of crystal.

The remainder of this section is devoted to a discussion of the second-order continuous spectrum. The continuum is due to a scattering process in which the light interacts with a pair of phonons in a single event, as illustrated in figure 8. We restrict our attention to the case where both phonons are created. There is now no restriction on the phonon wave vectors other than the requirement that their sum should balance the change in wave vector of the scattered photon. Subject to this condition, the phonon wave vectors can range over the entire Brillouin zone. Since the photon wave vectors are negligible compared to the Brillouin zone dimensions, wave vector conservation in this case requires effectively that the wave vectors of the two phonons should be equal and opposite. The continuous frequency distribution displayed by the scattered photons is thus proportional to a weighted density of lattice states in which two phonons of equal and opposite wave vector are present.

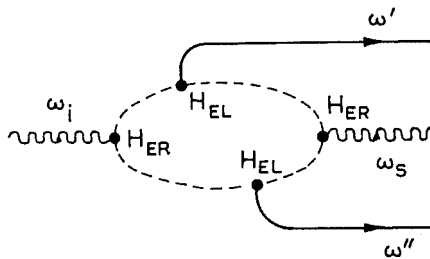


Figure 8. Elementary scattering process for the second-order continuous spectrum.

The weighting is due to the frequency and wave vector dependence of the interactions involved in the scattering process. The second-order continuous spectrum results from a single scattering event and the scattering efficiency is therefore independent of the crystal size, as in the first-order Raman effect. This fact leads to an experimental means for resolving the second-order line and continuous spectra in cases where the continuum has sharp features or where the lines are broad

The formal theory of the scattering efficiency for the second-order Raman effect can be tackled by the same methods as the first-order Raman effect. The first complete theoretical treatment was given by Born and Bradburn (1947), who applied their method to explain the experimental spectrum of NaCl. The same method was later applied to diamond by Smith (1948). The Born and Bradburn calculation of the second-order Raman effect is exactly analogous to their calculation of the first-order effect outlined in §2.2. The scattered intensity is related to the electronic polarizability tensor, which must now be expanded as far as terms proportional to a product of two nuclear displacement amplitudes, i.e. the second-order Raman effect results from the term of order r^2 in (23). The final result of the general calculation can be cast in a form for the scattering efficiency at Raman shift ω analogous to (29), but with the square of the polarizability derivative replaced by complicated simultaneous summations over the squares of the polarizability second derivative components and over phonon pairs whose frequencies ω' and ω'' add to give ω . In the applications of the general theory to NaCl and diamond it was assumed for simplicity that only products of the nuclear displacements of nearest neighbours contribute to the second-order term in the electronic polarizability expansion, and that the dominant contribution to the density of states arises from the region of the Brillouin zone close to the centre of the hexagonal face. As a result of these approximations each pair of phonon branches makes a contribution to the second-order continuum intensity at frequency shift ω equal to the combined density of states of the two branches at frequency ω multiplied by a proportionality factor which is constant for a given pair of branches. In this way Born and Bradburn (1947) and Smith (1948) were able to extract some quantitative results from the general theory and show that Born's theory of lattice dynamics is able to account for the main features of the distribution of intensity in the second-order Raman spectra of NaCl and diamond.

It would also be possible to calculate the Raman scattering efficiency by treating the four-step scattering process illustrated in figure 8 by fourth-order perturbation theory, similar to the treatment of first-order scattering which follows from (30). This calculation has however not been carried out and neither has the Born, Bradburn and Smith type of calculation been repeated during the period under review. Nevertheless, some progress has been made in the understanding of the structure in second-order Raman spectra in the last few years. This is largely due to advances in the theory of phonon densities of states, reviewed in the next section.

3.2. *Two phonon density of states and Raman selection rules*

Any structure which occurs in a second-order Raman spectrum reflects structure in the frequency dependence of the combined density of states of pairs of phonons with equal and opposite wave vector, or in the frequency dependence of the interaction which gives rise to the transition. Information about the structure of a phonon density of states can be obtained by means of an approach known as a critical-point analysis. When this information is combined with selection rules, it is

possible to interpret the shape of the second-order continuous Raman spectrum. This approach is simpler to carry through than a Born and Bradburn type of calculation, and it correlates experiment and theory in a way not possible by the older method. Although only partial critical-point analyses of Raman spectra have so far been made, the method appears to hold great promise and we review it briefly.

For the sake of simplicity we restrict the discussion to the case of cubic crystals having two atoms in the unit cell (e.g. diamond, rocksalt, zinc blende) and thus six phonon branches. A critical-point analysis determines the amount and nature of the structure in the single- or two-phonon density of states. Consider first the single-phonon density of states. Let \mathbf{k} be the phonon wave vector and $\omega(\mathbf{k})$ its frequency. A critical point is a point in \mathbf{k} -space where every component of $\nabla_{\mathbf{k}}\omega(\mathbf{k})$ is either zero or changes sign discontinuously. The importance of critical points arises from the circumstance that a plot of phonon density of states against frequency may exhibit a discontinuity of slope at a critical point. This property of critical points was first investigated by Van Hove (1953) and his work was later extended by Phillips (1956) (see also the review article by Maradudin *et al.* 1963). By making use of the methods of these authors, it is possible to locate all the slope discontinuities which occur in the single-phonon density of states, and to decide their shape. Some of the shapes which a slope discontinuity can have are illustrated by Loudon and Johnson (1964, table 2).

The discussion so far has been in terms of the single-phonon density of states. The critical-point method has been extended to deal with the two-phonon density of states by Loudon and Johnson (1964). We consider only the part of the second-order Raman spectrum due to lattice states in which two phonons are created. Since $\omega(\mathbf{k}) = \omega(-\mathbf{k})$, the relevant two-phonon density of states is obtained from two-phonon dispersion curves constructed by adding together all pairs of phonon branches at each wave vector \mathbf{k} . At each \mathbf{k} on the two-phonon dispersion curves constructed in this way the total wave vector of the two-phonon states is effectively zero, and every state is Raman active as far as the wave vector conservation rule is concerned. For six single-phonon branches there are 21 two-phonon branches, and their critical points and accompanying density of states slope discontinuities can be treated in exactly the same way as the corresponding phenomena on single-phonon branches. One can thus obtain a knowledge of the positions and shapes of all the slope discontinuities in the two-phonon density of states. The density of states histograms which result from lattice dynamics calculations are not sufficiently fine grained to show the critical points reliably, and the Born and Bradburn (1947) and Smith (1948) Raman spectrum calculations consequently do not display any sharp structure.

Most of the critical points in the phonon spectra occur at points of high symmetry in the Brillouin zone. Indeed Phillips (1959) has shown that for lattices based on the face-centred cubic structure (which includes diamond, rocksalt and zinc blende) critical points must occur on all phonon branches at the symmetry points Γ , X , L and W (we use here the notation of Bouckaert *et al.* 1936). This holds for both the single- and the two-phonon branches. The remaining critical points can occur on lines or planes of symmetry or at general points in the zone. As mentioned above, the structure of the observed Raman spectrum is influenced by the frequency dependence of the interactions involved as well as by the frequency dependence of the two-phonon density of states. The interactions are unlikely to have a frequency

dependence sufficiently rapid to introduce additional discontinuities in slope of the type occurring in the density of states. However, where second-order Raman scattering accompanied by creation of a particular phonon pair, corresponding to a critical point in the two-phonon spectrum, is a forbidden process, the effect of the discontinuous change of slope in the density of states is quenched, and the measured spectrum should show no discontinuity. It is thus important to have selection rules at particular \mathbf{k} -vectors for the pairs of phonon branches which can contribute to the second-order Raman effect.

The selection rules are simplest to calculate for the second-order line spectrum, where both phonons have effectively zero wave vector, and for the part of the second-order continuum due to $\mathbf{k} = 0$ phonons. The requisite group theory has been given by Bhagavantam and Venkatarayudu (1939). There is a slight distinction between a case where the two phonons belong to the same branch, and the two-phonon state is an *overtone*, and where they belong to different branches, and the two-phonon state is a *combination*. For combination states the Raman transition is allowed if the Kronecker product of the irreducible representations of the two phonons contains irreducible representations in common with the polarizability tensor. For overtone states, the symmetrized Kronecker square of the phonon irreducible representation must be formed to determine the selection rule. As explained in the previous section, the second-order scattering gives rise to a line if both phonons are active in first-order scattering, otherwise it forms part of the continuum. Several general rules follow in an obvious way for the second-order line spectrum. In a crystal possessing inversion symmetry, only odd-parity states can be electric-dipole active and only even states can be Raman active. The $\mathbf{k} = 0$ phonons have a well defined parity and thus no first- or second-order Raman line can possibly also occur in the crystal's absorption spectrum, and a rule of mutual exclusion applies. Also, the symmetrized Kronecker square of every $\mathbf{k} = 0$ irreducible representation contains the identity representation, and a component of the polarizability tensor always transforms by the identity representation. The overtones of all $\mathbf{k} = 0$ phonons are therefore Raman active.

Selection rules for the second-order continuous spectrum due to phonons with non-zero wave vector are in principle calculated in exactly the same way as outlined above. However, the phonon wave vector \mathbf{k} now ranges over the entire Brillouin zone and in calculating the selection rules it is necessary to form Kronecker products and symmetrized Kronecker squares of space-group irreducible representations corresponding to all \mathbf{k} -vectors. General methods for this type of calculation have been developed by Birman (1962). Although the mechanics of the calculation are basically the same as for $\mathbf{k} = 0$ phonons, the actual manipulations are more complex due to the higher dimensionality of the representations involved and the fact that more than one group of \mathbf{k} enters. Even in crystals possessing inversion symmetry, the phonons having non-zero wave vector do not in general have a well-defined parity and the rule of mutual exclusion breaks down. It can however be shown that the two-phonon overtone at a general wave vector is Raman active. Detailed selection rules for second-order Raman scattering have been tabulated for the diamond and zinc blende structures by Birman (1963), for diamond by Loudon and Johnson (1964) and for the rocksalt structure by Burstein *et al.* (1964).

The selection rule calculation also provides information about the state of polarization of the scattered radiation in the second-order Raman effect. Consider for example scattering from a cubic crystal with the experimental geometry of figure

6 for $\phi = 0$, and unpolarized incident light. The pair of phonons which collaborate to produce the second-order scattering generate a Kronecker square or product representation, whose reduction contains a sum of $\mathbf{k} = 0$ representations. For Raman activity this sum must contain one of the $\mathbf{k} = 0$ irreducible representations listed in the table. The A and E representations are associated with zero depolarization ρ and the F representation with non-zero ρ . The second-order Raman-scattered light thus has ρ non-zero or zero according as the sum of $\mathbf{k} = 0$ representations does or does not contain F. Values of ρ for particular phonon pairs have been tabulated by Loudon and Johnson (1964) for diamond, and by Burstein *et al.* (1964) for rocksalt. Birman (1963) has tabulated depolarizations for scattering by powdered crystals of diamond and zinc blende structure. These depolarizations for the second-order continuum are difficult to measure experimentally since the scattering at a particular frequency is usually due to several different pairs of phonons from a variety of branches and having a variety of \mathbf{k} -vectors.

Armed with a critical-point analysis and a set of selection rules, one is in a position to understand and interpret the second-order Raman spectrum. This type of interpretation has not so far been fully carried out, although the corresponding analysis for the infra-red absorption spectra of diamond-structure semiconductors has been successfully completed. For the Raman effect, some tentative interpretations of features in the measured spectra in terms of pairs of phonons at critical points have been given by Loudon and Johnson (1964) for diamond and by Burstein *et al.* (1964) for some of the rocksalt-structure alkali halides. The power of critical-point interpretations will increase as lattice dynamics calculations and Raman spectrum measurements improve.

At this point mention must be made of the method of Raman spectra interpretation used by Raman himself (see Raman 1956a for a recent exposition). In Raman's theory, the linear dimension of the unit cell is taken to be twice that assumed by other workers. This leads to a unit cell having eight times the normal volume, and hence a Brillouin zone having one-eighth the volume usually derived. The resulting total dimensionality of phonon branches at $\mathbf{k} = 0$ is now $6 \times 8 = 48$ for lattices of diamond or rocksalt symmetry. In the usually accepted Brillouin zone, six of these phonon branches are at Γ , 18 are at the three X points and 24 are at the four L points. In Raman's theory it is further assumed that only $\mathbf{k} = 0$ phonons and their overtones and combinations can produce scattering. In the theory used by other workers, this is tantamount to assuming that only phonon pairs at Γ , X and L can contribute to second-order Raman scattering. Since important critical points usually occur at Γ , X and L , Raman's assumption may sometimes be a good one and he and his co-workers have met with some success in interpreting features of the second-order spectra. In diamond, Raman's 48 $\mathbf{k} = 0$ phonon modes have nine distinct frequencies (including one zero-frequency acoustic branch). Using Raman's approach, Venkatarayudu (1954) has shown that the rule of mutual exclusion breaks down for second-order Raman scattering by the phonons which are at symmetry point X in the usual picture. This is in agreement with selection rules given by Birman (1963). The Raman theory predicts a second-order spectrum consisting of a limited number of discrete lines, rather than the continuous and line spectra predicted by the Born theory outlined above. Raman's views have not received any substantial acceptance outside India.

3.3. Experimental results

3.3.1. Diamond

Apart from the alkali halides, diamond is the only crystal for which a fairly complete measurement of the second-order Raman spectrum has been made, although there are some fragmentary results for other crystals. Second-order spectra have been published by Krishnan (1946b, 1947b) and the interpretation of the observed features has been the subject of much discussion. In the work of Smith (1948), already mentioned, the distribution of intensity in the second-order Raman spectrum of diamond was interpreted in terms of a weighted density of two-phonon states. Her calculation was challenged by Krishnan (1948), who regarded the entire second-order spectrum as being composed of discrete lines, and who presented a rival interpretation in terms of Raman's theory of lattice dynamics. This theory of the second-order spectrum has been further elaborated by Raman (1956b). More recently Loudon and Johnson (1964) have given selection rules for the second-order Raman effect in diamond and have compared the positions of features in the spectrum with the phonon frequencies at critical points deduced from absorption measurements by Hardy and Smith (1961) (see also the absorption measurements by Raman 1962). The phonon frequencies in diamond are not well established and any critical-point interpretation of the Raman spectrum can only be tentative. There is also room for improvement in the experimental results. Part of the second-order spectrum is obscured by one of the subsidiary mercury vapour lamp emission lines, which is scattered in the crystal without change of frequency. This difficulty could perhaps be avoided by the use of a laser source instead of the mercury lamp. For use in theoretical interpretations, the results of second-order Raman experiments are best presented as plots of scattered intensity against frequency, instead of direct plots of micro-photometer traces. Some of Krishnan's original measurements have been replotted on an intensity scale by Narayanan (1951).

A second-order Raman line occurs in diamond at twice the frequency shift of the first-order line. The elementary process which gives rise to the second-order line is illustrated in figure 7, and the scattering efficiency can be calculated by sixth-order perturbation theory using an extension of the method of §2.2 for the first-order scattering efficiency. The second-order scattering efficiency S_2 is not simply equal to the square of the first-order scattering efficiency S_1 (the same quantity as S given by (31)) because the photon which is present in the intermediate state of figure 7 is a virtual one and there is no energy conservation in this state. The result of a calculation of the second-order scattering efficiency S_2 , assuming the same geometry as in (29) and (31) is:

$$\frac{S_2}{S_1} = \frac{S_1}{Ld\Omega} \frac{V\epsilon\omega_1^2}{9\pi^2c^2} f\left(\frac{\omega_1}{\omega_g}\right), \quad (72)$$

where ω_g is the frequency of the forbidden electronic energy gap and all the other symbols are as previously defined. The function f has a complicated dependence on ω_1/ω_g and has an order of magnitude 10^{-2} for the experimental situation in diamond. The dependence of S_2 on the crystal volume, already discussed in §3.1, is evident in (72). An experimental value for the ratio S_2/S_1 has been measured by Krishnan and Narayanan (1950) to be $1/270$. They do not state all the dimensions of their diamond crystal, but their numerical result appears to be roughly consistent with the theoretical estimates of $S_1/Ld\Omega$ given earlier.

3.3.2. Alkali halides

Both the NaCl and CsCl alkali halide structures have two atoms in the unit cell and optic modes of negative parity at zero wave vector. They therefore have no first-order Raman effect and no second-order line spectrum. However, many of the alkali halides give a strong second-order continuous Raman spectrum. Among the NaCl-structure alkali halides, the second-order spectra of LiCl, NaCl, NaBr, NaI, KCl, KBr, KI and RbBr have been measured, and MgO can also be included in this group since it has the same structure. Among the CsCl-structure alkali halides, CsBr and CsI have been measured. References to the more recent of these measurements are listed in a separate group at the end of the article. The references for some of the older measurements can be found in the review article by Menzies (1953).

The first theoretical interpretation of a second-order Raman spectrum was made by Born and Bradburn (1947) using the measurements on NaCl by Krishnan (1945). A better measurement of the NaCl second-order Raman spectrum was subsequently made by Welch *et al.* (1949). Burstein *et al.* (1964) have given selection rules for second-order Raman scattering by pairs of critical-point phonons in the NaCl lattice and have shown that nearly all the observed features in the spectrum of Welch *et al.* can be accounted for as sums or differences of four characteristic phonon frequencies. By comparison with a lattice dynamics calculation for NaCl by Hardy and Karo (1960) it appears that the four important critical-point phonons are those at the symmetry point X . Raman (1961) has interpreted the NaCl spectrum in terms of his own theory of lattice dynamics.

The phonon frequencies in NaI and KBr have been measured by neutron spectroscopy for the important symmetry directions by Woods *et al.* (1963). Burstein *et al.* (1964) have shown that the majority of the features in the Raman spectra of these two crystals can be accounted for by combinations of phonon frequencies at symmetry points in the Brillouin zone given by the neutron scattering measurements.

Complete interpretations of the Raman spectra of the alkali halides must await sufficiently accurate lattice dynamics calculations or sufficiently detailed neutron spectroscopy measurements for full critical-point analyses to be carried through, following the lines indicated in §3.2.

4. Raman scattering other than by phonons

Raman scattering from crystals is normally associated with the creation or destruction of phonons, and the article has so far been exclusively concerned with this type of scattering. However, other types of crystal excitation can in principle produce Raman scattering. In this section we review the proposals which have been made for Raman scattering experiments involving four different types of crystal transition; only the first one has so far been observed experimentally.

4.1. Electronic states

Elliott and Loudon (1963) have proposed Raman scattering from paramagnetic ions in crystals as a useful method for determining the low-lying ionic energy levels, and Hougén and Singh (1963, 1964) have observed this type of Raman scattering from Pr^{3+} ions in PrCl_3 . Electronic Raman scattering had previously been observed in the x-ray region by Das Gupta (1959, 1962). The scattering efficiency for a process in which an ion is excited from an initial state with energy E_i to a final state with

energy E_f is easily derived from the theory of Heitler (1954) for atomic Raman scattering to be:

$$S = \frac{N}{V} \frac{e^4 \omega_s L d \Omega}{m^4 \omega_i c^4} \left| \sum_j \left\{ \frac{\mathbf{e}_i \cdot \mathbf{p}_{ij} \mathbf{e}_s \cdot \mathbf{p}_{jf}}{E_j - E_i - \hbar \omega_i} + \frac{\mathbf{e}_s \cdot \mathbf{p}_{ij} \mathbf{e}_i \cdot \mathbf{p}_{jf}}{E_j - E_i + \hbar \omega_s} \right\} \right|^2. \quad (73)$$

Here N/V is the number of paramagnetic ions per unit volume, and the remaining symbols all have their previously defined meanings. The summation j runs over all electronic intermediate states.

Numerical estimates on the basis of (73) indicate that, depending on the matrix elements and the positions of the excited intermediate states, the efficiency for electronic Raman scattering can be as large or larger than that for the lattice vibration Raman effect. This is the result for concentrated crystals where the paramagnetic ion under study is a normal constituent of the lattice so that $N/V \sim 10^{22}/\text{cm}^3$. For dilute crystals, where the paramagnetic ion is present as an impurity, the scattering efficiency is correspondingly smaller, although as Hougen and Singh point out, the sharpening of the electronic levels as the paramagnetic ions are diluted offsets the reduction in the integrated scattering intensity to some extent.

The selection rules and angular dependence of the electronic Raman scattering depend only on the symmetries of the initial and final states, and the results of the table can be used for electronic states. For ions which are situated at a lattice point having inversion symmetry, Raman scattering measures the energy separations between two states having the same parity (the lower state will normally be the ground state). In the rare-earth ions the initial and final states arise from the $4f^n$ configuration and the most important intermediate states will be of opposite parity and are expected to be from the $4f^{n-1}5d$ configuration. It is not clear from the work of Hougen and Singh to what extent this type of Raman effect experiment can supplement the knowledge of rare-earth energy levels obtained from the more conventional absorption and fluorescence measurements.

4.2. Spin waves

Two different mechanisms for Raman scattering by spin waves have been proposed. Bass and Kaganov (1960) have treated the process where the spin system of a ferromagnet is coupled directly to the radiation field by the magnetic-dipole interaction. Consider a cubic crystal with incident radiation parallel to the direction of saturation magnetization M_s which is taken to be the z axis. The scattering mechanism depends on the fact that the x and y components of the magnetization are linear in the spin-wave creation and destruction operators, whereas the z -component includes quadratic terms in the operators (see for example Van Kranendonk and Van Vleck 1958, equation (11)). The Raman effect for spin-wave creation proceeds as follows. 1. An incident photon, interacting only with the x and y components of the magnetization, is destroyed and an intermediate spin-wave quantum is created. 2. A scattered photon is created, via its interaction with the z -component of the magnetization, accompanied by destruction of the intermediate spin wave and creation of the final spin-wave quantum. Obviously the scattered radiation must make a finite angle ψ with the z -axis in order to be non-vanishing. The scattering efficiency for this process is:

$$S = \frac{(g\beta)^3 M_s \epsilon^2 \omega_i \omega_s (n_0 + 1) L d \Omega \sin^2 \psi}{2 \hbar^2 c^4}, \quad (74)$$

where g is the g -factor of the spins, β is the Bohr magneton and n_0 is now the spin-wave population. The spin-wave dispersion curve is essentially flat with frequency ω_0 at the wave vectors of interest, and $\omega_s = \omega_i - \omega_0$. For the anti-Stokes component of the scattering $n_0 + 1$ is replaced by n_0 , and $\omega_s = \omega_i + \omega_0$.

Bass and Kaganov propose a scattering experiment using incident radiation of wavelength 1 mm, which leads to a typical right-angle scattering efficiency per unit length per unit solid angle of about $10^{-19} (n_0 + 1)$. This is very small, but the experiment might be feasible in the microwave region where powerful sources are available. It is not clear what advantages the experiment would have over an ordinary ferromagnetic resonance experiment (ω_0 typically corresponds to a wavelength of order 1 cm).

Elliott and Loudon (1963) have pointed out that the existence of spin-orbit interaction in magnetic crystals leads to a mechanism for Raman scattering from spin waves. Consider a crystal containing magnetic ions whose ground states have quenched angular momentum, and spin S . The spin waves are made up from spin transitions on individual atoms, and a spin wave can be excited by a photon-scattering process of the type described by (73) where i and f now refer to the $S_z = S$ and $S_z = S - 1$ states of the ground multiplet of a single atom. In order to achieve a change in spin component as a result of two successive electric-dipole transitions it is necessary to have a mixing of spin and orbital states either in the ground state or in one of the intermediate excited states j , and this results in an extra factor of order $\lambda/(E_j - E_i)$ (spin-orbit splitting/configuration splitting) in the matrix element of (73). The estimated scattering efficiency for optical radiation is about 10^{-5} to 10^{-6} , but would be comparable with that resulting from Bass and Kaganov's mechanism if microwave radiation were used.

At small wave vectors the spin-wave frequency ω_0 in an anti-ferromagnet is given by $\hbar\omega_0 \approx (2JK)^{1/2}$, where J is the exchange energy and K is the anisotropy energy. For some anti-ferromagnets this corresponds to a wavenumber in the range 10 – 100 cm^{-1} where ordinary absorption measurements are difficult. Raman shifts of this magnitude can however be measured without too much difficulty at optical frequencies. Some ferrimagnets have 'optical' spin-wave branches with frequencies of the same order which should also be accessible to this type of measurement. The selection rules for the symmetry types of spin wave which can cause Raman scattering are discussed by Elliott and Loudon. The method could not be used for ferromagnetic spin waves, as the shifts would be too small to detect easily at optical frequencies.

4.3. Superconductors

Superconducting crystals possess a forbidden energy gap in their electronic spectra when they are cooled below the transition temperature. The breadth of the forbidden gap is typically in the range 10 – 30 cm^{-1} and it gives rise to an absorption edge which can be studied by far infra-red spectroscopy (Richards and Tinkham 1960). The gap can in principle also be detected and measured by a Raman scattering experiment, the scattered light occurring in a continuous distribution with Raman shifts greater than or equal to the gap frequency. The skin effect allows the incident light to penetrate only a very small distance into the superconductor (of order

10^{-5} cm) and the Raman frequencies must be sought in the light which is scattered from the specimen surface. This greatly reduces the scattered intensity available for detection and Khaikin and Bykov (1956) have made an unsuccessful attempt to measure Raman-scattered light from a superconducting lead film. The theory of this type of scattering has subsequently been worked out by Abrikosov and Fal'kovskii (1961), who estimate a scattering efficiency of order 10^{-13} or smaller for the process. The detection of this small fraction of the incident light intensity at optical frequencies represents a formidable experimental problem and a sensitivity at least 10^5 times that of Khaikin and Bykov would be required.

4.4. *Plasmons*

The Raman scattering of incident radiation by plasmons has been treated theoretically by Sobel'man and Feinberg (1958), but no experiments have been reported. Plasmons normally have frequencies well above the optical range and the frequency of the exciting radiation must be even higher than the plasma frequency. The experiment has the advantage that plasma modes which are inactive in direct absorption of radiation could be detected by their Raman effect.

5. Recent developments

5.1. *Use of lasers as Raman sources*

Raman scattering from lattice vibrations is a weak effect and a powerful sharp-line source of radiation is required in order that its detection should be feasible. Most experiments have used mercury vapour lamp sources whose strongest line occurs at a wave number 39420 cm^{-1} , and with three moderately strong lines two orders of magnitude less intense at wave numbers 24710 , 22950 and 18310 cm^{-1} . If the incident and scattered radiation is not to be absorbed in a crystal due to the excitation of electronic transitions across the forbidden energy gap, then the gap must be wider than about 2.3 eV , and preferably wider than about 5 eV so that the strongest of the mercury lines can be used ($1\text{ eV} = 8066\text{ cm}^{-1}$). Thus a wide range of crystals has been excluded from study by Raman effect experiments. In particular, there have been no Raman effect measurements of lattice vibration frequencies in semi-conducting crystals.

These experimental restrictions are likely to be relaxed by use of the optical and near infra-red masers (lasers) recently developed. These are powerful single-line sources which emit radiation either in very intense short pulses, or continuously with a smaller intensity comparable to that of the three moderately intense mercury lines. The pulse repetition frequency of the former variety of laser may be quite high, e.g. 1000 times per second. The scattered intensity in the Raman effect is proportional to the incident intensity, and since the spectrum is usually recorded photographically, the only requirement on the source is that its output integrated over a convenient exposure time should be sufficiently large. The high intensity of the low repetition frequency pulsed laser may thus be offset by the short pulse duration, and high peak power is not necessarily an advantage for a Raman source (see however the following section). Continuous wave and high repetition frequency pulsed lasers may prove to be the more useful Raman sources. Using a pulsed source, photo-electric detection of the scattered light using a cut-out on the detector between pulses seems to be a promising technique. This type of detection has been previously used by Valentin (1957) who employed a pulsed mercury lamp as his Raman source. The

laser possesses the advantage as a Raman source that its emission spectrum may consist of a single line or at worst a very small number of lines. In contrast, the mercury vapour lamp has a large number of emission lines, so that the Raman scattered light originating from an intense mercury line is often partly obscured by light originating from a weaker line scattered without change of frequency. This is the case for example in the second-order Raman spectrum of diamond (Krishnan 1964b).

Lasers have so far been used mainly as sources for the Raman spectroscopy of liquids. Porto and Wood (1962) have used a pulsed ruby laser source in this way, and more recently Kogelnik and Porto (1963) have employed a helium–neon laser. In unpublished work, some observations of the Raman spectra of ruby and CaF_2 have been made using laser sources. It seems likely that the Raman spectra of many crystals will be measured for the first time in the next few years as the technology and availability of lasers are improved.

5.2. Stimulated Raman effect

In the ordinary Raman effect, the scattered radiation is emitted *spontaneously* in directions distributed anisotropically over the complete 4π solid angle. Thus in calculating the time constant for Raman scattering in (30), the number of scattered photons at frequency ω_s in the initial state of the system was set equal to zero. The intensity of the scattered beam in the ordinary Raman effect is small, having characteristically 10^{-6} or 10^{-7} times the intensity of the incident beam. Observations are normally made at right angles to the incident beam to exclude from the spectrograph as much as possible of the radiation at frequency ω_i .

If the incident light beam is made sufficiently intense, scattered photons may be produced sufficiently fast for the number n_s of photons in the crystal having frequency ω_s and specified direction to become significant. This may be allowed for in the theory, and leads to the result that the expression for $1/\tau$ is multiplied by an extra factor $(n_s + 1)$. The unit term corresponds to the original spontaneous scattering, while the term proportional to n_s corresponds to a stimulated emission of scattered photons. Stimulated Raman scattering requires intense incident radiation and has been observed only with the use of high-power pulsed ruby laser sources. The first observation was made by Woodbury and Ng (1962) in Raman scattering from nitrobenzene, and most of the subsequent experiments have been on liquids. However, Eckhardt *et al.* (1963) have observed stimulated Raman scattering from crystals of diamond, calcite and α -sulphur, and other crystals will doubtless show the effect. Chiao and Stoicheff (1964) have made more detailed measurements on calcite.

Stimulated Raman effect experiments have been carried out either with the scattering sample inside the optical cavity of the laser or with the sample outside the cavity and the laser beam focused to increase its photon density. In the former case, the scattered radiation builds up coherently in the cavity, the most favourable direction for \mathbf{k}_s being perpendicular to the end mirrors of the cavity so that the scattered beam can be successively amplified by feedback effects as it re-passes through the Raman sample. Using a focused laser beam, no feedback occurs and the stimulated Raman photons can in principle be emitted from the crystal in all directions consistent with symmetry requirements. However, only the part of the sample which is illuminated by the laser is effective in producing and amplifying the radiation at frequency ω_s . The focused laser beam is very narrow, and its path length in the Raman sample is generally arranged to be as long as possible. The greatest intensity of scattered radiation is produced in those directions where the path length

of the scattered photons through the effective part of the crystal is greatest. Thus even when the Raman sample is outside the laser cavity, the majority of stimulated scattered radiation emerges from the sample in, or close to, the forward direction. The scattering efficiency in a typical stimulated Raman effect experiment is much higher than in the ordinary or spontaneous Raman effect, and values as high as 10^{-1} for the ratio of scattered to incident intensity have been reported. The high intensity of the Raman beam makes possible its spectroscopic resolution from the laser beam, even though their directions are the same.

The first suggestion for a stimulated Raman effect experiment in the optical region using a crystal scatterer was made by Zeiger and Tannenwald (1963). They considered the case of stimulated Raman scattering from electronic states of impurity ions in crystals. The corresponding spontaneous scattering experiment has been treated in §4.1. Let us consider the theory of the experiment for the case where the scattering crystal is inside the laser cavity and where the scattered radiation builds up in a single mode of the cavity having an angular frequency width which is small compared to the width 2Γ of the Raman line observed in spontaneous scattering. In addition to the extra factor $(n_s + 1)$ in the scattering probability per unit time, the sum over scattered photons whose wave vector direction lies within a solid angle $d\Omega$ must be replaced by the contribution of the single cavity mode excited. Assuming that the cavity mode has a frequency equal to that of the centre of the Lorentzian Raman line, then the strength of the scattering into the mode is proportional to $1/\Gamma$. The result of the calculation of Zeiger and Tannenwald (1963) for the stimulated part of the scattering probability per unit time can be written:

$$\frac{1}{\tau_{\text{stim}}} = \left(\frac{S}{Ld\Omega} \right) \frac{8\pi^2 c^4}{\omega_s^2 \Gamma \epsilon^2} \frac{n_i n_s}{V}, \quad (75)$$

where S is given by (73). If the z -coordinate is measured parallel to the axis of the laser cavity, the equations describing the attenuation of the flux ρ_i of incident photons and the growth of the flux ρ_s of scattered photons are:

$$-\frac{d\rho_i}{dz} = \frac{d\rho_s}{dz} = \frac{\rho_i \rho_s V}{\lambda c}, \quad (76)$$

where

$$\rho_i = \frac{n_i c}{V \epsilon^{1/2}}, \quad \rho_s = \frac{n_s c}{V \epsilon^{1/2}}, \quad \frac{n_i n_s}{\lambda} = \frac{\epsilon}{c \tau_{\text{stim}}}. \quad (77)$$

If the front face of the crystal is at $z = 0$ and ρ_i^0 and ρ_s^0 are the values of ρ_i and ρ_s at this point, then the solution of (76) for ρ_s is:

$$\rho_s = \rho_s^0 \left(1 + \frac{\rho_i^0 z V}{c \lambda} \right) + O(z^2). \quad (78)$$

If L is the length of the crystal and R_s is an effective reflection coefficient which takes account of all losses from the radiation at frequency ω_s , then the criterion for the stimulated Raman effect to occur is

$$\frac{\rho_i^0 V L}{c \lambda} > 1 - R_s. \quad (79)$$

Zeiger and Tannenwald (1963) have evaluated this criterion for various impurities in a range of host lattices and find that the production of stimulated Raman radiation

in this type of experiment should be feasible. No successful experiments have however been reported.

The analogous calculation for stimulated Raman scattering from lattice vibrations has been carried out by Loudon (1963a). Consider for example a diamond crystal in the same scattering geometry as described above. If a principal axis of the crystal coincides with the z -axis, then the stimulated part of the scattering probability per unit time is:

$$\frac{1}{\tau_{\text{stim}}} = \frac{2\pi^2 e^4 n_i n_s}{\hbar^3 m^4 d^2 M \epsilon^2 \Gamma \omega_s^2 \omega_0} [|R_{xy}^z|^2 + |R_{yx}^z|^2]. \quad (80)$$

The scattered radiation is thus unpolarized for unpolarized incident radiation, and the phonons produced have longitudinal polarization. There is no proportionality to the phonon population function n_0 in the above equation because of a cancellation between the Raman process and its inverse. Comparison with the equation analogous to (31) for the case of forward Raman scattering ($\psi = 0$ in figure 5) shows that (75) holds also for the case of stimulated Raman scattering from lattice vibrations, except that the quantity S refers to the corresponding spontaneous experiment at a low temperature where n_0 is negligible. Equations (76) to (79) also apply to scattering by lattice vibrations. Eckhardt *et al.* (1963) have observed stimulated Raman scattering from diamond. They see a strong Stokes line and a weaker line at twice the normal Stokes shift. This second line is caused by stimulated Raman scattering excited by the Stokes radiation. An anti-Stokes line was also observed in these experiments.

Stimulated Raman scattering from lattice vibrations in piezo-electric crystals can be treated in the same way. For the zinc blende lattice, reference to figure 1 shows that it is not possible to satisfy the wave vector conservation requirement (27) for forward scattering from transverse phonons (this may no longer be true when photon dispersion due to the electronic states is taken into account). However, it is possible to have Raman scattering from the longitudinal phonons even when \mathbf{k}_i and \mathbf{k}_s point in the same direction. When the unpolarized incident light is propagated parallel to the principal z -axis of the crystal, the stimulated scattering probability per unit time is given by (75), but with S replaced by the S_l of (52) for $n_l = 0$ (the equality of R_{xy}^z and R_{yx}^z has been used at this point). There have been no experimental observations of stimulated Raman scattering from zinc blende structure crystals.

The theory of stimulated Raman scattering from lattice vibrations in uniaxial crystals has been considered by Loudon (1963a). Both the incident and scattered radiation can have either ordinary or extraordinary polarization, leading to a variety of ways in which the wave vector conservation requirement (27) can be satisfied. The dependence of phonon and photon frequencies on crystal orientation leads to the possibility of obtaining stimulated radiation at a range of frequencies ω_s as the crystal is rotated. The phonons produced in this type of experiment would lie in general on the parts of the dispersion curves in figures 2 and 3 where the crystal excitation is partly electromagnetic and partly mechanical in character. There is some confusion in this region between the processes of stimulated Raman effect and optical parametric amplification, and a consideration of the theory would lead us somewhat outside the scope of the article. The interplay between the Raman effect and parametric amplification has been considered theoretically by Butcher *et al.* (1964).

References

- ABRIKOSOV, A. A., and FAL'KOVSKII, L. A., 1961, *Soviet Phys.—JETP*, **13**, 179.
- BASS, F. G., and KAGANOV, M. I., 1960, *Soviet Phys.—JETP*, **37**(10), 986.
- BHAGAVANTAM, S., 1953, *Proc. Indian Acad. Sci. A*, **37**, 350.
- BHAGAVANTAM, S., and VENKATARAYUDU, T., 1939, *Proc. Indian Acad. Sci. A*, **9**, 224.
- BIR, G. L., and PIKUS, G. E., 1961, *Soviet Phys.—Solid State*, **2**, 2039.
- BIRMAN, J. L., 1959, *Phys. Rev.*, **115**, 1493; 1962, *Ibid.*, **127**, 1093; 1963, *Ibid.*, **131**, 1489.
- BLOUNT, E. I., 1963, *Solid State Physics*, **13**, 305.
- BORN, M., and BRADBURN, M., 1947, *Proc. roy. Soc. A*, **188**, 161.
- BORN, M., and HUANG, K., 1954, *Dynamical Theory of Crystal Lattices* (Oxford: Clarendon Press).
- BOUCKAERT, L. P., SMOLUCHOWSKI, R., and WIGNER, E., 1936, *Phys. Rev.*, **50**, 58.
- BRILLOUIN, L., 1922, *Ann. Phys., Paris*, **17**, 88.
- BURSTEIN, E., JOHNSON, F. A., and LOUDON, R., 1964, *Phys. Rev.* (to be published).
- BUTCHER, P. N., LOUDON, R., and MCLEAN, T. P., 1964, *Proc. phys. Soc. Lond.* (to be published).
- BUTCHER, P. N., and MCLEAN, T. P., 1963, *Lasers and Applications*, Edited by W. S. C. Chang (Ohio State University Press), p. 173.
- CHANDRASEKHARAN, V., 1963, *Z. Phys.*, **175**, 63.
- CHIAO, R., and STOICHEFF, B. P., 1964, *Phys. Rev. Letters*, **12**, 290.
- COCHRAN, W., and COWLEY, R. A., 1962, *J. Phys. Chem. Solids*, **23**, 447.
- COUTURE-MATHIEU, L., KETELAAR, J. A. A., VEDDER, W., and FAHRENFORT, J., 1952a, *Physica*, **18**, 762; 1952b, *J. chem. Phys.*, **20**, 1492.
- COWLEY, R. A., 1962, *Phys. Rev. Letters*, **9**, 159.
- DARWIN, C. G., 1934, *Proc. roy. Soc. A*, **146**, 17.
- DAS GUPTA, K., 1959, *Phys. Rev. Letters*, **3**, 38; 1962, *Phys. Rev.*, **128**, 2181.
- DAYAL, B., 1950, *Proc. Indian Acad. Sci. A*, **32**, 304.
- ECKHARDT, G., BORTFELD, D. P., and GELLER, M., 1963, *Appl. Phys. Letters*, **3**, 137.
- EHRENREICH, H., 1957, *J. Phys. Chem. Solids*, **2**, 131.
- ELLIOTT, R. J., and LOUDON, R., 1963, *Physics Letters*, **3**, 189.
- GRECHKO, L. G., and OVANDER, L. N., 1962, *Soviet Phys.—Solid State*, **4**, 112.
- HAAS, C., 1956, *Spectrochim. Acta*, **8**, 19.
- HAAS, C., and HORNIG, D. F., 1957, *J. chem. Phys.*, **26**, 707.
- HARDY, J. R., and KARO, A. M., 1960, *Phil. Mag.*, **5**, 859.
- HARDY, J. R., and SMITH, S. D., 1961, *Phil. Mag.*, **6**, 1163.
- HEINE, V., 1960, *Group Theory in Quantum Mechanics* (Oxford: Pergamon Press).
- HEITLER, W., 1954, *The Quantum Theory of Radiation* (Oxford: Clarendon Press).
- HERZBERG, G., 1945, *Infra-red and Raman Spectra of Polyatomic Molecules* (New York: D. Van Nostrand).
- HOUGEN, J. T., and SINGH, S., 1963, *Phys. Rev. Letters*, **10**, 406.
- HUANG, K., 1951, *Proc. roy. Soc. A*, **208**, 352.
- KETELAAR, J. A. A., HAAS, C., and FAHRENFORT, J., 1954, *Physica*, **20**, 1259.
- KHAIKIN, M. S., and BYKOV, V. P., 1956, *Soviet Phys.—JETP*, **3**, 119.
- KLEINMAN, D. A., and SPITZER, W. G., 1962, *Phys. Rev.*, **125**, 16.
- KOGELNIK, H., and PORTO, S. P. S., 1963, *J. opt. Soc. Amer.*, **53**, 1446.
- KONDILENKO, I. I., KOROTKOV, P. A., and STRIZHEVSKII, V. L., 1960, *Optics and Spectroscopy*, **9**, 13.
- KONDILENKO, I. I., and STRIZHEVSKII, V. L., 1961, *Optics and Spectroscopy*, **11**, 137.
- KRISHNAN, R. S., 1948, *Proc. Indian Acad. Sci. A*, **28**, 307.
- LAX, M., and BURSTEIN, E., 1955, *Phys. Rev.*, **97**, 39.
- LOUDON, R., 1963a, *Proc. phys. Soc., Lond.*, **82**, 393; 1963b, *Proc. roy. Soc. A*, **275**, 218.
- LOUDON, R., and JOHNSON, F. A., 1964, *Proc. roy. Soc. A*, **281**, 274.
- LYDDANE, R. H., SACHS, R. G., and TELLER, E., 1941, *Phys. Rev.*, **59**, 673.
- MARADUDIN, A. A., 1962, *Phys. Stat. Sol.*, **2**, 1493.
- MARADUDIN, A. A., and FEIN, A. E., 1962, *Phys. Rev.*, **128**, 2589.
- MARADUDIN, A. A., FEIN, A. E., and VINEYARD, G. H., 1962, *Phys. Stat. Sol.*, **2**, 1479.

- SiO₂, CaF₂, Al₂O₃, etc. (temperature dependence).
- BOBOVICH, YA. S., and BURSIAI, E. V., 1961, *Optics and Spectroscopy*, **11**, 69.
BaTiO₃.
- BRAHMS, S., and MATHIEU, J. P., 1960, *C.R. Acad. Sci., Paris*, **251**, 938.
HgCl₂.
- COUTURE-MATHIEU, L., and MATHIEU, J. P., 1953, *C. R. Acad. Sci., Paris*, **236**, 371.
ZnS (Zinc blende).
- COUTURE-MATHIEU, L., POULET, H., and MATHIEU, J. P., 1952, *C.R. Acad. Sci., Paris*, **234**, 1761.
NaClO₃ and NaBrO₃
- FLUBACHER, P., LEADBETTER, A. J., MORRISON, J. A., and STOICHEFF, B. P., 1959, *J. phys. Chem. Solids*, **12**, 53.
Vitreous silica (first order Raman and Brillouin).
- GEIGER, W., and KULP, M., 1960, *J. Phys. Chem. Solids*, **12**, 341.
Quartz glass (Brillouin scattering).
- GROSS, E., 1930, *Nature, Lond.*, **128**, 201
Quartz (Brillouin scattering).
- HADNI, A., HENRY, C., MATHIEU, J. P., and POULET, H., 1961, *C.R. Acad. Sci., Paris*, **252**, 1585.
Hg₂Cl₂
- HOUGEN, J. T., and SINGH, S., 1964, *Proc. roy. Soc. A*, **277**, 193.
PrCl₃ and LaCl₃ (electronic and vibrational).
- IKEGAMI, S., 1964, *J. phys. Soc., Japan*, **19**, 46.
BaTiO₃.
- KRISHNAMURTI, D., 1954, *Proc. Indian Acad. Sci. A*, **40**, 211.
Diamond
1956; *Proc. Indian Acad. Sci. A*, **43**, 210.
MgCO₃
1957, *Proc. Indian Acad. Sci. A*, **46**, 183.
CaCO₃ (calcite)
1958, *Proc. Indian Acad. Sci. A*, **47**, 276.
SiO₂ (quartz);
1962, *Proc. Indian Acad. Sci. A*, **55**, 290.
TiO₂ (rutile).
- KRISHNAN, R. S., 1946a, *Proc. Indian Acad. Sci.*, **24**, 45.
Diamond (temperature dependence)
1947a, *Nature, Lond*, **159**, 740; 1947b, *Proc. Indian Acad. Sci.*, **26**, 399.
Diamond (Brillouin scattering)
1953, *Proc. Indian Acad. Sci. A*, **37**, 377.
Fuzed quartz (first-order Raman and Brillouin);
1955, *Proc. Indian Acad. Sci. A*, **41**, 91.
Brillouin scattering (see §2.7.2).
- KRISHNAN, T. S., 1956, *Proc. Indian Acad. Sci. A*, **44**, 96.
SrCO₃
- KRISHNAN, R. S., and NARAYANAN, P. S., 1963, *Indian J. pure appl. Phys.*, **1**, 196.
BaF₂.
- MATHIEU, J. P., and COUTURE-MATHIEU, L., 1952a. *J. Phys. Radium*, **13**, 271.
ClO₄Li.3H₂O;
1952b, *C.R. Acad. Sci., Paris*, **234**, 1961.
SiO₂ (quartz);
1953, *J. Chim. Phys.*, **50**, 573.
CuCl₂
- MATHIEU, J. P., COUTURE, L., and POULET, H., 1955, *J. Phys. Radium*, **16**, 781.
K₂SO₄ and Li₂SO₄.
- MATHIEU, J. P., and POULET, H., 1957, *C. R. Acad. Sci., Paris*, **244**, 2794.
SiC (carborundum)
- MATHIEU, J. P., POULET, H., and KLEE, W., 1963, *Copenhagen Lattice Dynamics Conf. Abstracts*, p. 55.

- ZnS (wurtzite).
- MATHIEU, J. P., POULET, H., and TRAMER, A., 1960, *Z. Elektrochem.*, **64**, 699.
CuCl.
- MOSZYNSKA, B., 1963, *C.R. Acad. Sci., Paris*, **256**, 1261.
SnBr₄, SnCl₄ and TiCl₄.
- NARAYANAN, P. S., 1953, *Proc. Indian Acad. Sci. A*, **37**, 411.
TiO₂ (rutile).
- NARAYANAN, P. S., and VEDAM, K., 1961, *Z. Phys.*, **163**, 158.
SrTiO₃.
- NARAYANASWAMY, P. K., 1947, *Proc. Indian Acad. Sci. A*, **26**, 511, 521. Calcite and quartz
(temperature dependence).
- NEDUNGADI, T. M. K., 1940, *Proc. Indian Acad. Sci.*, **11**, 86.
Quartz (temperature dependence).
- PERSHINA, E. V., and RASKIN, SH. SH., 1962, *Optics and Spectroscopy*, **13**, 272.
AlCl₃ and AlBr₃.
- POULET, H., and MATHIEU, J. P., 1956, *J. Phys. Radium*, **17**, 472.
BeSO₄ · 4H₂O and NH₄H₂PO₄.
- REDING, F. P., and HORNIG, D. F., 1954, *J. chem. Phys.*, **22**, 1926.
NH₃ and ND₃.
- RICHMAN, I., 1964, *Phys. Rev.*, **133**, A1364.
SrF₂ and BaF₂.
- RICHMAN, I., SATTEN, R. A., and WONG, E. Y., 1963, *J. chem. Phys.*, **39**, 1833.
LaCl₃ and LaBr₃.
- SCROCCO, M., and MATHIEU, J. P., 1958, *Ann. Phys., Paris*, **3**, 463.
PbSO₄.
- SRINIVASAN, R., 1953, *Proc. Indian Acad. Sci. A*, **37**, 405.
AlF₂SiO₄ (topaz).
- STEKHANOV, A. I., 1955, *C.R. Acad. Sci., U.S.S.R.*, **100**, 685.
Gypsum
1957, *Optika i Spektrosk.*, **3**, 143.
CaCO₃ (calcite) and BaSO₄.
- STEKHANOV, A. I., and CHISLER, E. V., 1962, *Soviet Phys.—Solid State*, **3**, 2549.
SiO₂, CaCO₃ and CaF₂ (temperature dependence).
- STEKHANOV, A. I., and GABRICHIDZE, Z. A., 1963, *Soviet Phys.—Solid State*, **5**, 972.
Rochelle salt.
- TRAMER, A., 1959a, *C.R. Acad. Sci., Paris*, **248**, 3546; 1959b, *Ibid.*, **249**, 2531.
NaNO₂.
- WEIL, A., and MATHIEU, J. P., 1954, *C.R. Acad. Sci., Paris*, **238**, 2510.
Mg and Zn perchlorates.
- ZUBOV, V. G., and OSIPOVA, L. P., 1961, *Soviet Phys.—Crystallography*, **6**, 330.
Quartz
1962, *Soviet Phys.—Doklady*, **7**, 525.
Quartz (neutron irradiated).
- ZUBOV, V. G., OSIPOVA, L. P., and FIRSOVA, M. M., 1962, *Soviet Phys.—Crystallography*,
6, 623.
Quartz (electric field applied).

Second-order Raman Experiments

- KHAMBÁTÁ, S. J., 1956, *Proc. phys. Soc., Lond. A*, **69**, 426.
MgO.
- KRISHNAMURTHY, N., and KRISHNAN, R. S., 1963, *Indian J. pure appl. Phys.*, **1**, 239.
CsI
- KRISHNAN, R. S., 1945, *Nature, Lond.*, **156**, 267.
NaCl
1946b, *Proc. Indian Acad. Sci.*, **24**, 25.
Diamond.
- KRISHNAN, R. S., and KRISHNAMURTHY, N., 1963, *Z. Phys.*, **175**, 440.
NaI

- KRISHNAN, R. S., and NARAYANAN, P. S., 1949, *Nature, Lond.*, **163**, 570.
 KBr
 1950, *Proc. Indian Acad. Sci. A*, **32**, 352.
 Diamond.
- KRISHNAN, R. S., and NARAYANAN, P. S., 1957, *J. Indian Inst. Sci. A*, **39**, 85.
 KI.
- NARAYANAN, P. S., 1955, *Proc. Indian Acad. Sci. A*, **42**, 303.
 CsBr.
- RAMAN, C. V., 1963, *Proc. Indian Acad. Sci. A*, **57**, 1.
 KBr
- STEKHANOV, A. I., and ELIASHBERG, M. B., 1961a, *Optics and Spectroscopy*, **10**, 174;
 1961b, *Soviet Phys.—Solid State*, **2**, 2096.
 KBr and KBr–KCl mixed crystals.
- STEKHANOV, A. I., GARBRICHIDZE, Z. A., and ELIASHBERG, M. B., 1961, *Soviet Phys.—Solid State*, **3**, 964.
 KI
- STEKHANOV, A. I., and KOROL'KOV, A. P., 1963, *Soviet Phys.—Solid State*, **4**, 2311.
 CsBr
- STEKHANOV, A. I., KOROL'KOV, A. P., and ELIASHBERG, M. B., 1962, *Soviet Phys.—Solid State*, **4**, 945.
 LiCl
- WELSH, H. L., CRAWFORD, M. F., and STAPLE, W. J., 1949, *Nature, Lond.*, **164**, 737.
 NaCl.

Recent Publications

The following list of publications, with descriptions of their contents, brings the references up to date at the time of proof-reading (end of October 1964).

- AXE, J. D., 1964, *Phys. Rev.*, **136**, A42. Develops method for approximate numerical evaluation of (73), §4.1, and compares the theoretical predictions with the results of Hougén and Singh (1963, 1964).
- CHIAO, R. Y., TOWNES, C. H., and STOICHEFF, B. P., 1964, *Phys. Rev. Letters*, **12**, 592. Measurements of *stimulated Brillouin scattering* from quartz and sapphire using a ruby laser source (cf. §§2.7 and 5.2).
- COWLEY, R. A., 1964, *Proc. phys. Soc., Lond.*, **84**, 281. Contains shell-model theory of Raman scattering, with numerical calculations of the second-order spectra of NaI and KBr.
- HOBDEN, M. V., and RUSSELL, J. P., 1964, *Phys. Letters* (to be published). First and second-order Raman spectra of GaP using a He–Ne laser as the source. This is the first published crystalline Raman spectrum using a laser source (cf. §5.1).
- KLEINMAN, D. A., 1964, *Phys. Rev.*, **134**, A423. It is shown that a measurement of the Raman spectrum of the F-centre could provide important new information about the centre.
- KONDILENKO, I. I., VERLAN, E. M., KOROTKOV, P. A., and STRIZHEVSKII, V. L., 1963, *Soviet Phys.—Solid State*, **5**, 1158. Contains theory of the variation of Raman intensity with scattering angle for uniaxial crystals, and a comparison with experiments on the 466 cm^{-1} vibration of quartz (cf. §§2.3. and 2.4).
- LUBCHENKO, A. F., and PAVLIK, B. M., 1963, *Soviet Phys.—Solid State*, **5**, 1246. Theory of Raman and Rayleigh scattering from impurity molecules in crystals.
- POULET, H., and MATHIEU, J. P., 1964a, *C.R. Acad. Sci., Paris*, **258**, 2043; 1964b, *Ann. Phys., Paris* (to be published). The Raman frequencies of CdS excited by the green and yellow Hg lines are tabulated and interpreted.
- RUSSELL, J. P., 1964, *Proc. phys. Soc., Lond.* (to be published). First and second-order Raman spectra of CaF₂ excited by a He–Ne laser (cf. §2.6.3).
- STRIZHEVSKII, V. L., 1963, *Soviet Phys.—Solid State*, **5**, 1099. Discusses a polarizability-theory approximation for the Raman scattering tensor in crystals (cf. §2.2).
- WARRIER, A. V. R., and KRISHNAN, R. S., 1964, *Naturwissenschaften*, **51**, 8: First-order Raman shift of SrF₂ measured to be 285 cm^{-1} (cf. §2.6.3).